The Astronomical Journal, 131:1163–1183, 2006 February

THE TWO MICRON ALL SKY SURVEY (2MASS)

M. F. Skrutskie,[1,2] R. M. Cutri,[3] R. Stiening,[1] M. D. Weinberg,[1] S. Schneider,[1] J. M. Carpenter,[4]
C. Beichman,[5] R. Capps,[5] T. Chester,[3] J. Elias,[6] J. Huchra,[7] J. Liebert,[8] C. Lonsdale,[3]
D. G. Monet,[9] S. Price,[10] P. Seitzer,[11] T. Jarrett,[3] J. D. Kirkpatrick,[3] J. E. Gizis,[1]
E. Howard,[1] T. Evans,[3] J. Fowler,[3] L. Fullmer,[3] R. Hurt,[3] R. Light,[3,12]
E. L. Kopan,[3] K. A. Marsh,[5] H. L. McCallon,[3]
R. Tam,[3] S. Van Dyk,[3] and S. Wheelock[3]

Received 2004 September 27; accepted 2005 September 30

ABSTRACT

Between 1997 June and 2001 February the Two Micron All Sky Survey (2MASS) collected 25.4 Tbytes of raw imaging data covering 99.998% of the celestial sphere in the near-infrared J (1.25 μm), H (1.65 μm), and K_s (2.16 μm) bandpasses. Observations were conducted from two dedicated 1.3 m diameter telescopes located at Mount Hopkins, Arizona, and Cerro Tololo, Chile. The 7.8 s of integration time accumulated for each point on the sky and strict quality control yielded a 10 σ point-source detection level of better than 15.8, 15.1, and 14.3 mag at the J, H, and K_s bands, respectively, for virtually the entire sky. Bright source extractions have 1 σ photometric uncertainty of <0.03 mag and astrometric accuracy of order 100 mas. Calibration offsets between any two points in the sky are <0.02 mag. The 2MASS All-Sky Data Release includes 4.1 million compressed FITS images covering the entire sky, 471 million source extractions in a Point Source Catalog, and 1.6 million objects identified as extended in an Extended Source Catalog.

Key words: catalogs — infrared: general — surveys

1. INTRODUCTION

By 1990, astronomical infrared array technology had matured to enable a full-sky census with millijansky sensitivity and arcsecond resolution. The acute scientific need for such a census was highlighted in the astronomy decadal survey report (Bahcall et al. 1991) in which an all-sky near-infrared survey was identified as the top small-project priority for the coming decade. The design and execution of the Two Micron All Sky Survey (2MASS) has fulfilled this need by delivering uniform precise photometry and astrometry over the entire celestial sphere in the J (1.25 μm), H (1.65 μm), and K_s (2.16 μm) near-infrared photometric bands. 2MASS produced a Point Source Catalog containing 470,992,970 sources and an Extended Source Catalog of 1,647,599 sources, along with 4,121,439 FITS images covering 99.998% of the sky. These products along with several ancillary tables constitute the 2MASS All-Sky Data Release[13] made available to the public in 2003 March. This paper describes the 2MASS hardware and data collection system, pipeline data reduction software, and the general nature and quality of the 2MASS data products. It is not, however, a guide to the detailed characteristics of the 2MASS data products, nor is it a tutorial on the productive scientific use of the catalogs and images. The 2MASS Explanatory Supplement (Cutri et al. 2003) fulfills these roles.

2. SURVEY FACILITIES AND INSTRUMENTATION

2.1. *Survey Design and Requirements*

Wavelength coverage is a primary attribute of any full-sky survey. 2MASS was conceived as a ground-based near-infrared survey, and, as such, atmospheric transmission and ambient thermal background significantly constrained the choice of wavelength bands. The longest wavelength atmospheric window that is not severely compromised by thermal background emission is the classical K band defined by Johnson (1962) and first surveyed by Neugebauer & Leighton (1969). The project's name, 2MASS, derived from the desire to produce a complete and reliable survey at this longest wavelength accessible with good sensitivity from the ground: 2 μm.

Distinguishing the effects of interstellar extinction and delineating stellar and extragalactic populations requires at least three bandpasses. The two infrared atmospheric bandpasses immediately shortward of the K band, namely, J band (1.2 μm) and H band (1.6 μm), were natural choices for 2MASS. An alternative choice of I band (0.8 μm) paired with J band was rejected, despite its broader wavelength coverage, because observing these bands would have required a mixture of CCD and near-infrared array technologies.[14]

Science drivers, in tandem with practical constraints, dictated the sensitivity of 2MASS. With its ability to penetrate interstellar

[1] Department of Astronomy, University of Massachusetts, Amherst, MA 01003.
[2] Current address: Department of Astronomy, P.O. Box 3818, University of Virginia, Charlottesville, VA 22903-0818.
[3] Infrared Processing and Analysis Center, California Institute of Technology, Pasadena, CA 91125.
[4] Department of Astronomy, California Institute of Technology, Pasadena, CA 91125.
[5] Jet Propulsion Laboratory, Pasadena, CA 91109.
[6] National Optical Astronomy Observatory, Tucson, AZ 85726.
[7] Harvard-Smithsonian Center for Astrophysics, Cambridge, MA 02138.
[8] Department of Astronomy, University of Arizona, Tucson, AZ 85721.
[9] US Naval Observatory, Flagstaff Station, Flagstaff, AZ 86002.
[10] Air Force Research Laboratory, Hanscom Air Force Base, MA 01731.
[11] Department of Astronomy, University of Michigan, Ann Arbor, MI 48109.
[12] Deceased, 1998 May 20.
[13] See http://www.ipac.caltech.edu/2mass/releases/allsky/.

[14] At the time of the specification of the 2MASS project requirements the z band, now in common use owing to its implementation in the SDSS (Fukugita et al. 1996), was not in regular use as a photometric standard bandpass.

TABLE 1
2MASS Parameters and Point-Source Specifications

Parameter	Value
Arrays	256 × 256 NICMOS3 (HgCdTe)
Pixel size	2.″0
Wave bands	J, H, and K_s (2.00–2.31 μm)
Telescopes	1.3 m equatorial Cassegrain
Integration time	6 × 1.3 s per frame = 7.8 s total
	Specification/Goal
Sensitivity (S/N = 10)	15.8, 15.1, and 14.3 mag for J, H, and K_s, respectively
Photometric accuracy	5% for bright sources
Photometric uniformity	4% over the sky
Positional accuracy	0.″5 relative to ICRS
Completeness/reliability	0.99/0.9995

extinction and a unique sensitivity to cool objects, a near-infrared survey had the potential to discover new and rare objects, delineate the structure of the Milky Way, and establish the distribution of galaxies in nearly 4π sr with a minimal zone of avoidance. Discovering brown dwarfs required detection of <2000 K objects out to tens of parsecs. Probing Galactic structure necessitated detecting cool giant stars on the far side of the Galactic disk and in the halo to distances of 50 kpc. Meaningful observation of large-scale structure required completeness in the detection of galaxies with luminosity, L_*, to $z = 0.05$. All of these objectives imply 5 σ near-infrared sensitivities of order 1 mJy. This sensitivity level, constrained by the practical limitations of resources available to survey the sky in the mid-1990s, established the interplay of pixel size, array format, telescope size, and integration time.

Integration time per sky pixel in an all-sky survey scales almost directly with the number of camera pixels available in each band. An ideal survey instrument contains a large number of large-format arrays for each wavelength band (e.g., Sloan Digital Sky Survey [SDSS]; York et al. 2000). When 2MASS was proposed in the early 1990s, the only near-infrared array format reliably available in quantity was 256×256 pixels. Given the complexities associated with optomechanical design and data acquisition for systems with multiple arrays per band and the risk incurred by requiring even the minimum six "science-grade" arrays, a 2MASS focal plane format of 256×256 pixels per band was well constrained.

Given 256×256 pixels per exposure and reasonable assumptions about the amount of clear time at likely survey sites, the choice of pixel angular scale and integration time dictate the total duration of a full-sky survey. The realities of large project funding set a maximum operational lifetime for 2MASS of a few years. A three year survey with $2'' \times 2''$ pixels permits integration times of several seconds on each independent sky pixel. Larger pixels sacrifice resolution and enhance confusion at low Galactic latitudes. Smaller angular pixel scales lengthen the survey duration unless exposure times become so short that read noise dominates the Poisson noise from terrestrial airglow and thermal background.

2MASS selected a $2.''0 \times 2.''0$ pixel scale with 7.8 s of integration devoted to each sky location. Since background Poisson noise would dominate the system read noise in exposures of more than 1 s, even in the low-background J band, this total integration time was divided into six 1.3 s exposures. In addition to improving reliability, this redundant imaging enabled recovery of sky area that fell on nonfunctioning pixels and pixels affected by transient events such as cosmic rays and meteors. Multiple sampling also aided in overcoming the effects of undersampling, since the $2.''0 \times 2.''0$ pixel size was large compared with a typical 1″ FWHM seeing disc. Table 1 summarizes the basic parameters of 2MASS and performance objectives for point sources.

2MASS required telescope facilities in both the northern and southern hemispheres in order to observe the entire celestial sphere. Achieving millijansky sensitivity in the allotted integration time necessitated telescope apertures larger than 1 m. Existing telescopes could have been modified to serve the needs of 2MASS; however, the cost of modification was a significant fraction of the cost of new facilities. Furthermore, identical facilities would simplify operations and aid in the generation of a more uniform final product. At the time, 1.3 m diameter telescopes were the largest commercial telescopes that were in regular production and thus offered some economy of scale. Two identical 1.3 m aperture telescopes were constructed at Mount Hopkins, Arizona, and Cerro Tololo, Chile, for the sole purpose of carrying out 2MASS observations.

2.2. *Arrays, Cameras, and Bandpasses*

Each 2MASS camera contains three NICMOS3 256×256 HgCdTe arrays manufactured by Rockwell International Science Center, now Rockwell Scientific. These arrays have 40 μm pixel pitch and are sensitive between wavelengths of 0.8 and 2.5 μm. Two dichroic mirrors within each camera (Fig. 1) permit simultaneous imaging of an $8.'5 \times 8.'5$ field at a pixel scale of 2″ pixel^{-1} in the three 2MASS wave bands. These bands, defined primarily by interference filters, as well as by detector quantum efficiency, transmission/reflection losses at the system's optical surfaces, and the atmosphere, largely correspond to the classical J, H, and K bands defined by Johnson (1962), with the exception that the 2MASS "K-short" (K_s) filter excludes wavelengths longward of 2.31 μm to reduce thermal background and airglow and includes wavelengths as short as 2.00 μm to maximize bandwidth (Fig. 2).

A liquid nitrogen cryostat encloses all of the 2MASS optical elements and arrays with the exception of the ZnSe dewar entrance window. Milligan et al. (1996) describe the details of the 2MASS optical design and prescription. A cryogenic field stop lies at the f/13.5 telescope Cassegrain focal plane directly behind the dewar window. The field stop, located at the overlapping conjugate images of the arrays themselves, is slightly undersized relative to the array images in order to prevent light from scattering from the rough edge of the sapphire array substrate. The optical

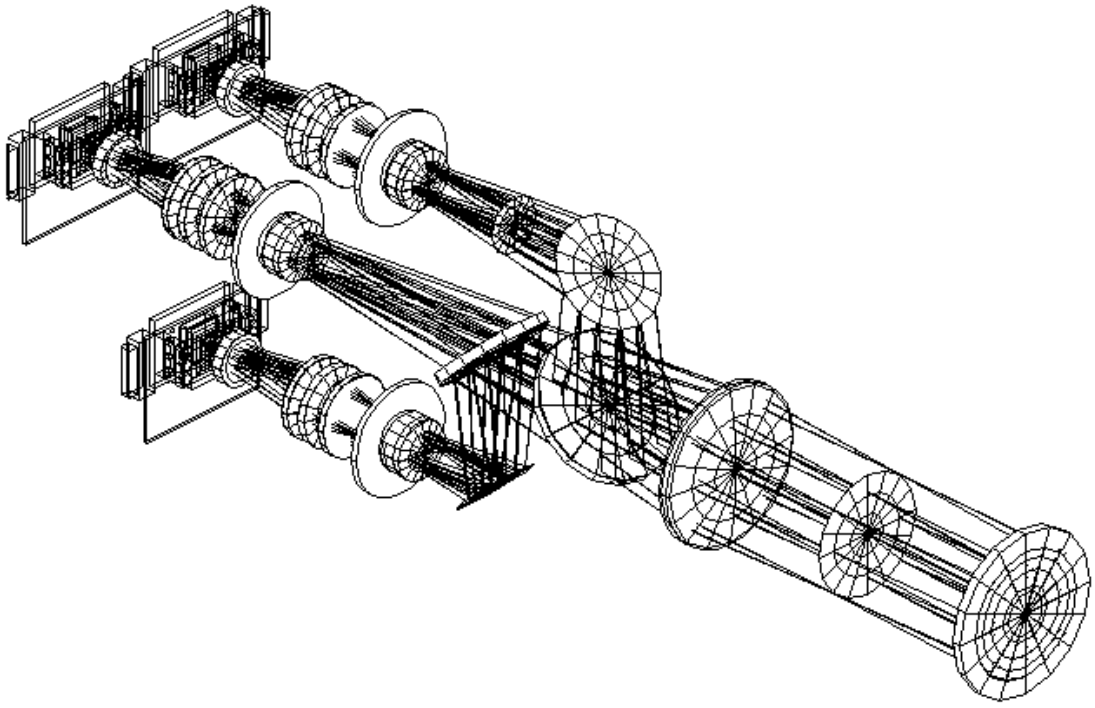

FIG. 1.—2MASS camera optics. Light enters through the ZnSe window at right. The Cassegrain focal plane lies 10 cm behind the window at a cryogenic field stop. A first lens is common to all three bands. Two dichroic mirrors immediately follow this common lens to split the light between the three bandpasses with the *J*-band light reflected first and the K_s-band light undeviated. Broadband filters near each Lyot stop primarily define the bands.

path to each array traverses seven lenses. The first Infrasil lens, common to all bands, relays nearly collimated light to beam-splitting mirrors. Following the beam splitters, the light for each band encounters independent identical sets of six lenses, which relay images of the sky onto the three arrays. These calcium fluoride and Infrasil lenses form pupil images at three Lyot stops adjacent to the band-limiting interference filters. The stop diameter is 90% of the pupil diameter to permit some freedom for misalignment of the three stops relative to one another. All lens surfaces are spherical and antireflection coated.

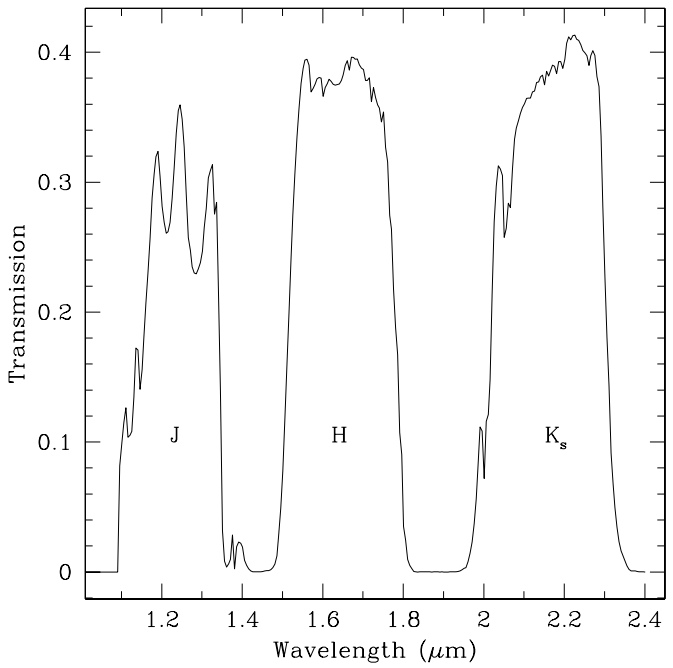

FIG. 2.—2MASS bandpasses. The curve represents calculated total transmission as a function of wavelength including the atmosphere (modeled with precipitable water = 5 mm), telescope optics, camera optics, and array quantum efficiency. This composite transmission is derived from witness measurements of mirror, dichroic, lens coating efficiency, and quantum efficiency measurements of similar arrays.

The three NICMOS3 arrays mount independently from the camera's optical support structure. Arrays can be translated in three dimensions with the system disassembled and warm, which enables the relative registration of the arrays to better than <200 μm, or $<10''$ on the sky. Two of the three arrays can be rotated about the optical axis with the system cold and mounted on the telescope. During the survey the arrays were rotated $\sim 0\overset{\circ}{.}3$ from the celestial coordinate system so that stars crossed one array column as they traversed the array in the declination direction in order to improve the sampling of stellar profile. The average plate scale for all six arrays (three northern and three southern) was $1\overset{''}{.}991$ pixel^{-1} with a maximum of $2\overset{''}{.}006$ pixel^{-1} (northern *H* band) and a minimum of $1\overset{''}{.}980$ pixel^{-1} (southern K_s band). Beginning as early as the start of northern operations in 1997 the northern *H*-band array began to experience pixel loss with each thermal cycle. Despite minimizing thermal cycling of the camera, this pixel loss began to threaten the redundant sampling of sources by 1999, and the *H*-band array was replaced. With the exception of the generation of new flat-fields and bad pixel maps, survey operations were transparent to this event. Even the *H*-band plate scale remained unchanged at $2\overset{''}{.}006$ pixel^{-1}. The replacement array operated through the completion of the survey.

During 2MASS, commercial readout electronics simultaneously clocked all four quadrants of all three arrays with a pixel dwell time of 3 μs. Pixel voltage was sampled to 16 bit precision. Analog-to-digital conversion gain was 8 e ADU $^{-1}$ with a typical readout noise level of 4.5 ADU in a doubly correlated difference image. In practice, Poisson noise from ambient

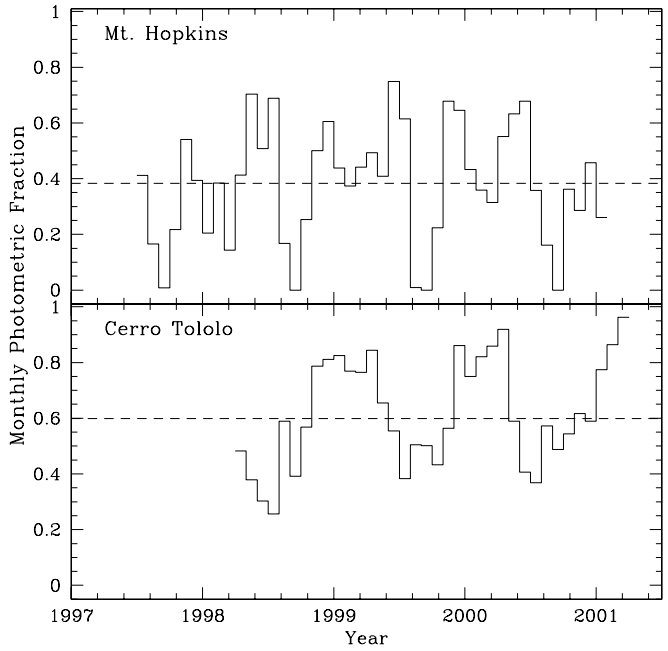

FIG. 3.—Monthly photometric fraction vs. time at the northern and southern observatories. The horizontal dashed lines represent the average nightly photometric fraction at each site (38% north and 60% south).

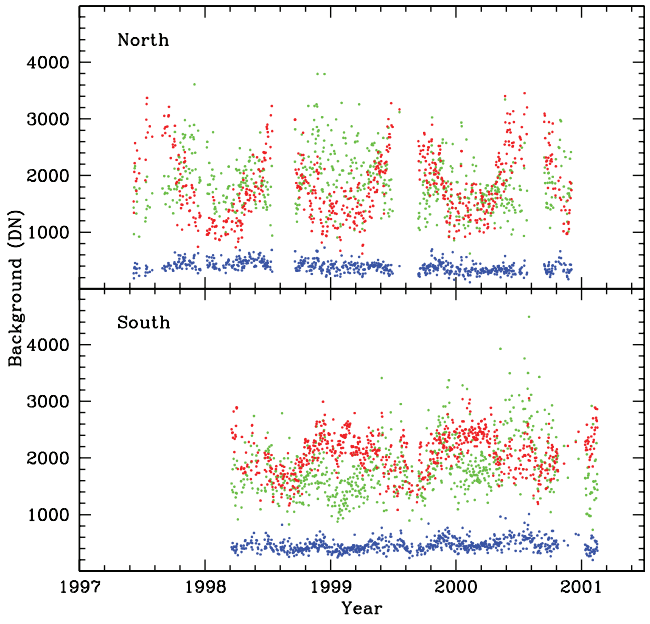

FIG. 4.—Mean nightly J (*blue*), H (*green*), and K_s (*red*) backgrounds vs. time for the two 2MASS observatories. Backgrounds at the J and H bands primarily arise from airglow. The K_s background depends on both airglow and thermal background and thus is seasonal.

background flux overwhelmed the electronic read noise. A complete readout of the array required 51 ms. The data system recorded two complete reads of the array: one immediately following the array reset and another 1.3 s later. The pixel-by-pixel difference between these two readouts constitutes a 1.3 s doubly correlated exposure. For 2MASS the array reset timing was identical to the timing for a readout. Thus, the first readout, although it occurred immediately after reset, captured a 51 ms exposure of the sky in each pixel. The 1.3 s duration exposures saturated for stars between 8–9 mag. The 51 ms exposure extended the unsaturated regime to sources as bright as 4–5 mag.[15]

2.3. *Telescopes*

2MASS used two custom 1.3 m equatorial telescopes. The northern telescope is located at the Whipple Observatory at 2306 m elevation on a ridge below the summit of Mount Hopkins, Arizona (N 31°40′50.″8, W 110°52′41″), while the southern telescope site is at Cerro Tololo Inter-American Observatory at 2171 m elevation on a ridge below the summit of Cerro Tololo, Chile (S 30°10′3.″7, W 70°48′18″). For each telescope, the primary mirror, composed of Corning ultra-low expansion glass, is parabolic with a radius of curvature of 5200 mm. The secondary conic constant is −1.847 with a radius of curvature of 965.7 mm. These optics provide a Cassegrain focal ratio of f/13.5 and a Cassegrain plate scale of 11.″97 mm^{-1}.

Invar rods establish the primary-secondary mirror separation and minimize thermal variation of the telescope focus. Calibration of focus change versus temperature during telescope commissioning permitted application of computed thermal focus corrections during survey observations. This automated thermal focus correction, amounting to 5 μm of secondary motion °C^{-1}, permitted observations to proceed for weeks without real-time feedback from the images. Seasonal adjustments of the focus zero point of order 10 μm accounted for any remaining focus residual at the largest temperature extremes.

2.4. *Observatory Site Conditions*

The 2MASS observing facilities operated every night that stars were visible and there was no threat of rain. Feedback from the data processing system provided statistics on background levels, seeing/image size, achieved sensitivity, and system zero point (total transmission). A modest weather station provided statistics on surface humidity, temperature, and barometric pressure with each observation. Figures 3–7 summarize the time history of some of these parameters for both hemispheres. Figure 3 shows the observed monthly fraction of photometric hours. The annual closure of the northern hemisphere facility during the Arizona summer monsoon is evident in the Mount Hopkins data. The dashed horizontal line represents the mean photometric fraction for each site. Figure 4 plots background in each band during the survey. Airglow emission dominates the J and H bands. Significant seasonal variation is apparent in the K_s-band background, since thermal emission from the telescope optics was usually comparable to or greater than the airglow emission in this band. Seasonal temperature variations were more mild at the Cerro Tololo site. Figure 5 tracks the image FWHM, which represents the convolution of the system point-spread function (PSF) with the seeing. The 2″ pixels, camera optics, and sampling pattern combined to produce a system PSF of 2.″5 under the best seeing conditions. Northern hemisphere image size improved during the first years of the survey due to the discovery and correction of a primary mirror support problem. Sensitivity at the signal-to-noise ratio S/N = 10 detection level (Fig. 6) was evaluated hourly from the statistics of the repeated scans of calibration tiles as described in § 3.4. Background, seeing, and atmospheric transparency were the primary factors that determined this sensitivity level. As a result, K_s-band sensitivity experienced significant seasonal change due to the

[15] The Point Source Catalog includes a *rd_flg* column that identifies the origin of the photometry for each band for a given source.

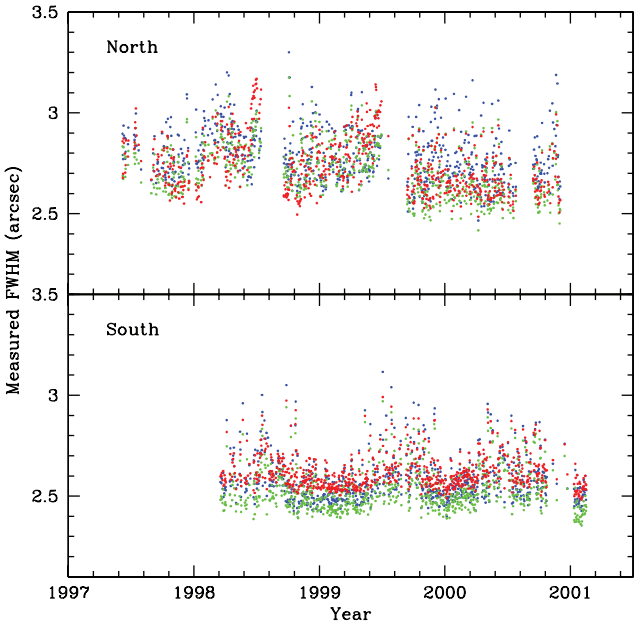

FIG. 5.—Mean nightly J (*blue*), H (*green*), and K_s (*red*) measured image FWHM intensity vs. time for the two 2MASS observatories.

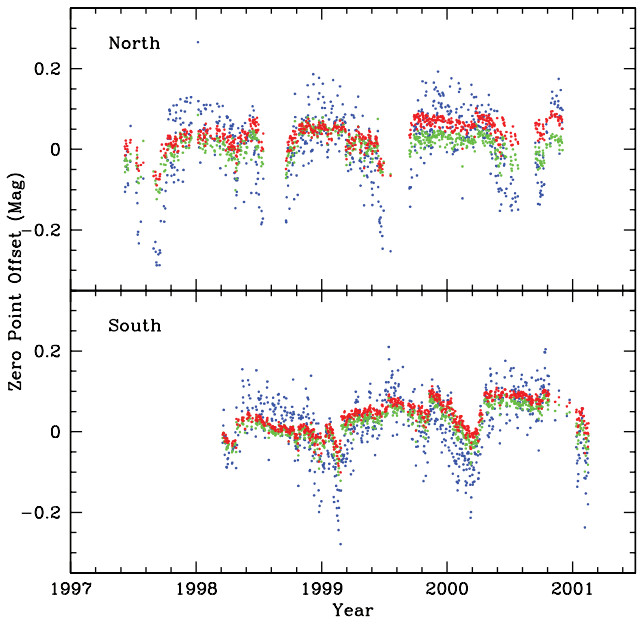

FIG. 7.—Mean nightly J (*blue*), H (*green*), and K_s (*red*) photometric zero points vs. time for the two 2MASS observatories. The zero point is measured in magnitudes and represents the offset between instrumental and calibrator magnitudes. The zero point thus tracks the total system transmission, with more negative values indicating poorer sensitivity.

variation in thermal background, while J and H band were less affected. Zero points (Fig. 7) represent the total system transmission including the Earth's atmosphere. Because the 2MASS J band infringes on atmospheric water absorption and is more susceptible to atmospheric scattering, significant seasonal variations in J-band zero point occurred during the survey. Not surprisingly, the worst transmission losses in the northern hemisphere occur at J band and are coincident with the start and end of the summer monsoon. Zero-point variations were removed from the derived source magnitudes via hourly observations of calibration fields (§ 3.4).

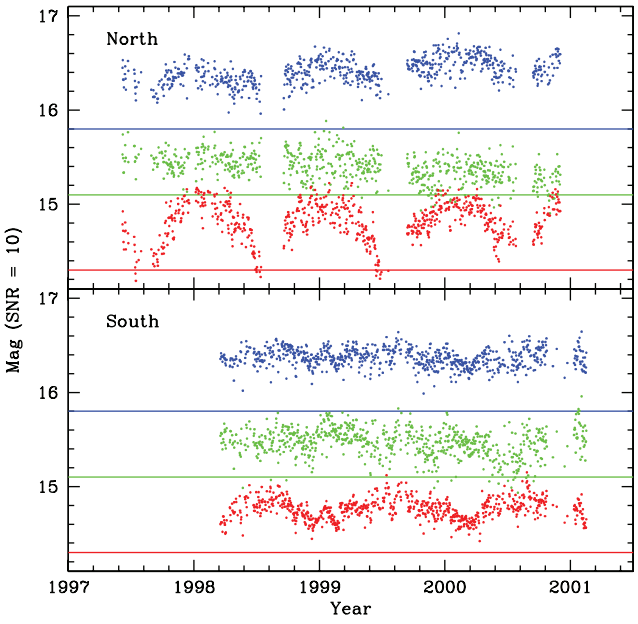

FIG. 6.—Achieved mean nightly J (*blue*), H (*green*), and K_s (*red*) S/N = 10 sensitivity levels in magnitudes vs. time for the two 2MASS observatories. This sensitivity is calculated from the statistics of repeated observations of stars in each set of hourly calibration observations. The solid horizontal lines represent the survey's S/N = 10 sensitivity requirement in each band: $J = 15.8$, $H = 15.1$, and $K_s = 14.3$.

3. DATA COLLECTION

3.1. *Data System Configuration*

Three personal computers controlled data acquisition, telescope pointing, and scheduling. A scheduling computer maintained a sky coverage database and selected regions of the sky for observation. The scheduling computer, via an RS-232 serial link, communicated requests for sky coverage to an instrument control computer. The instrument control computer, in turn, relayed requests for telescope motion to a telescope control computer and triggered camera frame acquisition. The instrument control computer also received, displayed, and stored the returned data. The scheduling computer could thus control a complete night of autonomous data acquisition. A telescope operator opened the facility and initiated the scheduling program. The operator then supervised the progress of observations and monitored the weather, closing the facility as required.

3.2. *Image Acquisition*

Observations proceeded while the telescope scanned steadily in declination at a rate of $57'' \text{ s}^{-1}$. During a 1.3 s exposure the secondary mirror tilted smoothly to freeze the $8\farcm5 \times 8\farcm5$ field of view relative to the focal plane despite the telescope's declination motion. Aberrations introduced by the secondary tilt were minimal compared with the system's PSF. At the end of a 1.3 s exposure the secondary rapidly tilted back to its start position, while the camera electronics read out and reset the arrays. The frame-to-frame time interval was 1.455 s, of which 1.351 s were used to collect data, with the remainder used for secondary flyback and array readout. The $57'' \text{ s}^{-1}$ scan rate thus produced an $83''$ spatial offset between frames—slightly smaller than one-sixth of the camera field of view—yielding six independent

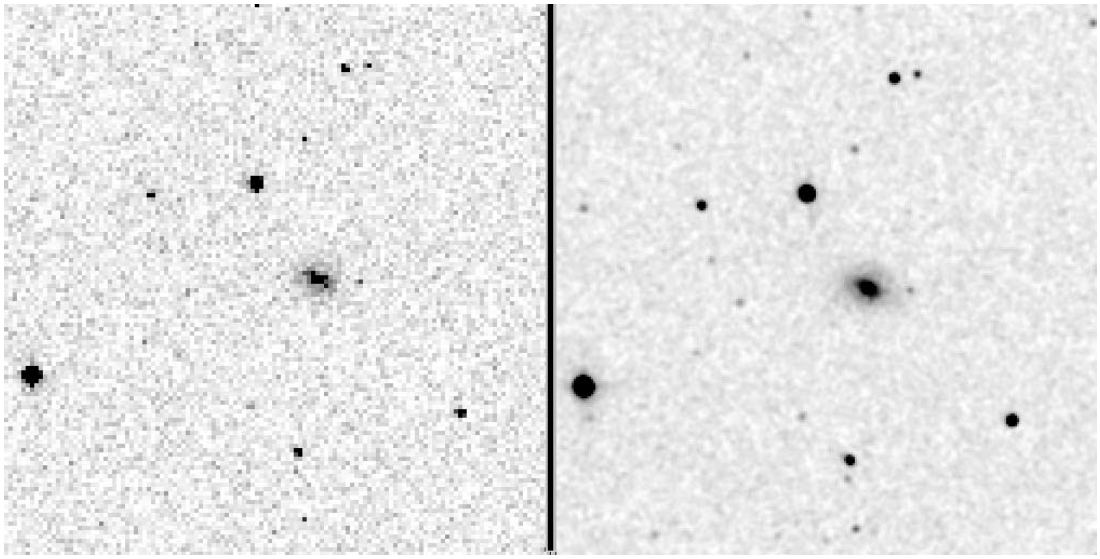

FIG. 8.—Comparison of a single 2MASS 1.3 s *J*-band exposure (*left*) to the Atlas Image (*right*), which is a kernel-smoothed composite of six 1.3 s exposures.

images of each sky position. Following each 1.3 s exposure the camera electronics transmitted six 256 pixel × 256 pixel × 16 bit frames (two images constituting the doubly correlated frames in each of the three bands) via a fiber optic interface to the instrument control computer, which displayed the images and stored them to hard disk. At the end of a full night of observations approximately 20 Gbytes of raw frame data were written to DLT tape. The tapes were subsequently express mailed to the Infrared Processing and Analysis Center (IPAC) for processing and archiving.

The 2MASS 2.″0 pixel size was large relative to the typical stellar image FWHM. The six independent images, appropriately distributed relative to pixel centers, mitigated undersampling effects. In the cross-scan direction (right ascension) subpixel stepping was achieved by rotating the arrays such that a given star crossed a full column while the source stepped down the array. Along the scan direction (declination) subpixel stepping was achieved by setting the telescope scan rate so that each step was a noninteger multiple of the pixel size. In practice, both of these adjustments were tuned to produce a well-distributed set of six centroids relative to the pixel grid for each star on each array. Since each array had a slightly different plate scale, only a limited range of step sizes and array rotations produced optimal results. The step size in declination was slightly different between the northern (82.″6 per step) and southern (82.″3 per step) hemisphere facilities.

Figure 8 compares a single 2MASS 1.3 s exposure to a final kernel smoothed image that incorporates information from the six dithered exposures. The figure demonstrates that the subpixel stepping produced stellar images that were smooth on scales smaller than the 2.″0 × 2.″0 pixels. Owing to the large pixel size, however, star images on the combined frames were large compared with a typical 1″ FWHM seeing disk. The best 2MASS images have FWHM of 2.″5 (Fig. 5). Spatial undersampling also degraded photometric precision for bright sources. The statistics of repeated observations of 2MASS calibration stars, discussed in § 5.2.4, demonstrate that the mean magnitude uncertainty for bright sources was typically 0.02 mag.

3.3. *Tiling Strategy and Scheduling*

2MASS defined a "scan" as a basic data unit. Scans consisted of 273 (northern site) or 274 (southern site) frames acquired as the telescope scanned steadily in declination. A scan covered a region of sky that was one 8.′5 camera field of view wide in right ascension and 6° long in declination. The celestial sphere was divided into 59,650 slightly overlapping predefined scan-sized survey "tiles." The scheduling software optimally selected a set of tiles and their order of observation each night. The scheduling program based its tile selection on accessibility near transit and, if a tile had been previously observed, a tile's priority for reobservation. The tiles were grouped by declination band: 0°–6°, 6°–12°, 12°–18°, etc. Tiles overlapped in the right ascension direction by 10% of their width (∼50″) at the tile end nearest the celestial equator. The convergence of lines of constant right ascension toward the pole produced increased tile overlap on the poleward end of each tile. Tiles extended a full camera frame (8.′5) in declination beyond the tile's designated declination boundary at the end closest to the celestial equator in order to overlap with the adjacent declination band. These various overlaps ensured that gaps would only rarely appear between adjacent tiles due to telescope pointing errors. The tile overlap also defined the maximum size of an extended source that always would appear entirely on the array in one or the other of two overlapping scans. The repeated observations of sources in the overlap regions provided substantial feedback on the photometric quality of the observations.

Northern hemisphere observations began in the 12°–18° declination band and proceeded northward. In the southern hemisphere, observations began in the 0° to −6° declination band and proceeded southward. The region between 0° and 12° was reserved for observation toward the end of survey operations since it could be observed from either hemisphere. Despite the shorter overall operational lifetime (35 vs. 42 months in the north), the southern facility observed 58% of the available tiles. Figure 9 delineates the sky coverage contributions of the two observatories to the Point and Extended Source Catalogs.

3.4. *Photometric Calibration*

2MASS observed photometric calibration tiles at regular intervals during each night. A calibration tile observation consisted of 48 consecutive frames obtained with the same scanning method and integration time as was used for the 6° scans. A scan of a calibration tile covered a field of view one camera frame wide

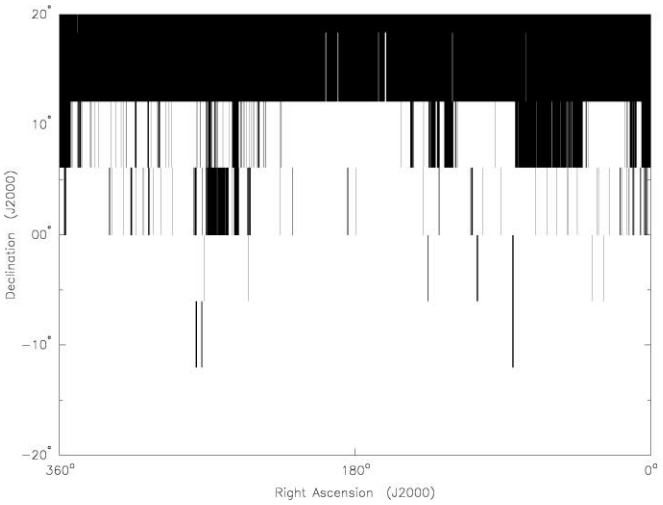

FIG. 9.—Sky coverage vs. facility. The declination range plotted covers the shared declination region observed by the two facilities. Tiles shown in black were observed by the northern hemisphere facility and incorporated into the All-Sky 2MASS data products.

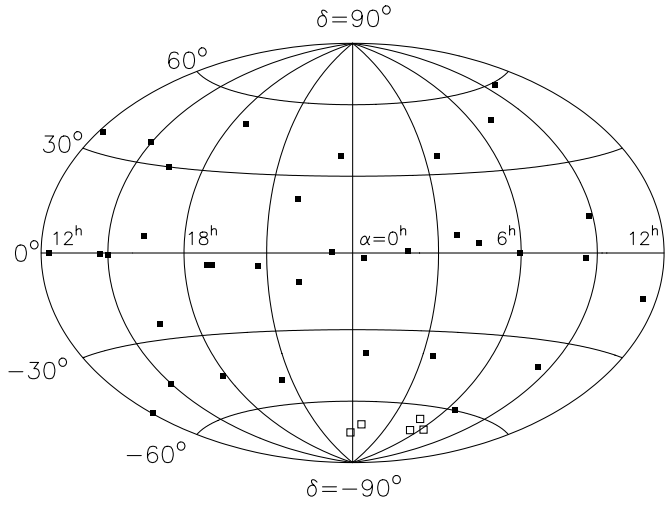

FIG. 10.—Distribution of 2MASS calibration tiles on the celestial sphere in equatorial coordinates. Filled squares are primary calibration tiles. Open squares denote additional calibration tiles created late in operations to support calibration of deep LMC and SMC observations.

(8.″5) in right ascension and 1° long in declination. Although each calibration tile was centered on a primary calibrator star (drawn largely from Near-Infrared Camera and Multi-Object Spectrometer [NICMOS] calibrators from Persson et al. [1998]), dozens of S/N > 20 stars within each calibration tile were used to estimate zero-point corrections.[16] A calibration observation consisted of six consecutive scans of a calibration tile, each requiring about 1 minute of elapsed time. The scan direction alternated between northward and southward, and each scan was offset 5″ in right ascension to mitigate any effects due to undersampling and bad pixels. Since each scan provided six images of each star, a 7 minute calibration observation acquired 36 independent 1.3 s images of every star in the tile. Subsequent processing reduced these images to six assessments of flux for each star—one from each of the six calibration scans.

Thirty-five calibration tiles were uniformly distributed around the sky (Fig. 10). The automated scheduling program selected several tiles for calibration each night, observing at least one tile at a variety of zenith angles. Equatorial calibration tiles were shared by both observatories. At the beginning of northern operations two calibration tiles were observed every 2 hr during the night. After 1997 October 11 the calibration strategy was modified so that one calibration tile was observed approximately every hour during a night. All southern calibration used the hourly strategy. Nightly 2MASS operations began and ended with a calibration observation. The scheduling software adjusted the time interval between calibration observations so that the final calibration observation occurred just prior to the onset of morning twilight. Calibration observations thus preceded and followed virtually all observations of 6° survey tiles. The consistency of the measured zero point within a set of six calibration observations, as well as consistency with zero points measured throughout the night, established whether conditions were photometric during a calibration observation. Calibration observations obtained both before and after a set of survey tile scans must have passed photometricity tests in order for the survey data to qualify as photometric.

Nightly calibration solutions (Fig. 11) were derived from linear fits to an entire night's data for H and K_s bands or from hour-to-hour interpolation for J band. These fitting functions were selected based on minimization of photometric dispersion in an analysis of the ensemble of all calibration data in which each individual calibration observation was treated, in turn, as if it were "survey" data. The J band experienced the largest overall variation in zero point, largely because the band's wavelength edges infringed on spectral regions of variable water vapor opacity. The hour-to-hour piecewise zero-point interpolation accommodated this short-term variability.

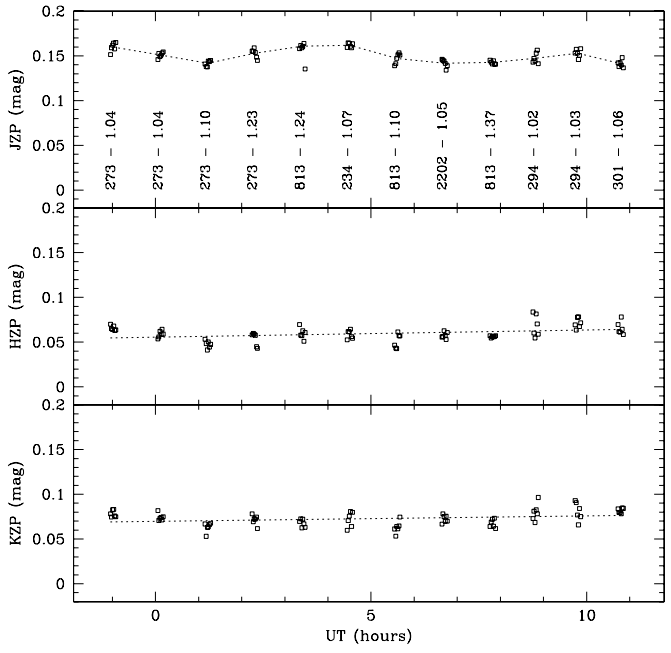

FIG. 11.—Typical 2MASS nightly calibration solution. The Y-axis represents the average zero-point (ZP) difference between the instrumentally derived magnitude and the calibrator magnitude for the ensemble of calibration standards in the tile. Clusters of points represent the six independent zero-point determinations from each of six successive observations of a 2MASS calibration tile. Each set of observations is labeled with the calibration tile identification number and the air mass at the time of observation. The J-band photometric solution is an hour-to-hour interpolation of the observed hourly mean zero points. The H-band and K_s-band solutions are linear fits to the entire night's data.

[16] The 2MASS Explanatory Supplement lists these target fields and calibration stars at http://www.ipac.caltech.edu/2mass/releases/allsky/doc/sec3_2d.tbl1.html.

Prior to final data processing the ensemble of all observations of photometric standards were solved for minimal photometric dispersion (Nikolaev et al. 2000), creating a network of 958 self-consistent and highly precise (residuals $\sim$0.01 mag) near-infrared standards. These standards[17] formed the basis for estimation of the hourly zero point. Atmospheric extinction is small [$<$0.10 mag (air mass)$^{-1}$] in the 2MASS bands and thus difficult to measure precisely on a nightly basis, since system zero-point variation can be similar to or larger than intranight extinction variations. Instead, each individual observation was corrected for extinction using the monthly extinction estimate from the global calibration analysis.

The 2MASS Point Source and Extended Source Catalogs report photometry in the natural 2MASS system. This system adopts the magnitudes reported in Persson et al. (1998) for the primary calibrator embedded in each of the 2MASS calibration tiles. Photometric zero points and absolute calibration of 2MASS are described in Cohen et al. (2003). Carpenter (2001) compared the colors of stars observed by both telescopes and found no significant differences in observed colors between the two observatories. Carpenter (2001) also derived empirical relations to transform data measured in a variety of other photometric systems to the 2MASS system. These color transformations, originally derived from early release data, have been updated in the 2MASS Explanatory Supplement to reflect the contents of the All-Sky data products.[18]

The 2MASS calibration data set includes thousands of independent observations of many calibration tiles. Each set of six calibration tile observations yields statistics on the sensitivity and S/N as a function of source magnitude for the instantaneous observing conditions that prevailed during that set of observations (§ 5.2.3). These statistics demonstrate that seeing and background were the primary factors determining the instantaneous sensitivity of a 2MASS observation. The sensitivity of any single survey scan could thus be established by referencing that scan's seeing and background in each band to the ensemble of calibration scan sensitivity statistics.

3.5. *Data Quality Feedback*

Optimal scheduling of tiles for observation required rapid assessment of image quality and photometric quality of the data. 2MASS developed a "24-hour" quality assurance monitor, which processed all calibration observations for a night within 24 hr of the receipt of a night's data at the IPAC processing facility. Calibration observations bracketed every hour-long interval of survey observations. If a calibration set indicated nonphotometric conditions or likely poor seeing, the adjacent survey tiles were triaged and marked as "unobserved" in scheduling priority.

Full nights of data were processed as quickly as possible, providing detailed tile-by-tile feedback on tile positioning, image FWHM, airglow, and sensitivity for tiles that were observed under otherwise photometric conditions. As these tiles were processed, each received a priority for reobservation based largely on the tile's derived sensitivity relative to the S/N = 10 sensitivity specification. For scheduling purposes, unobserved tiles took precedence over tiles with marginal sensitivity. In the end, 10,981 tiles were reobserved (18% of the sky) to improve on a previously marginal observation. Late in operations, 325 new tiles were created to cover small gaps left between observed tiles due to telescope pointing errors. Ultimately 99.998% of the sky was observed under photometric conditions. In all three bands 99.4% of the sky met or exceeded the S/N = 10 sensitivity requirement. Sensitivity was degraded by about 0.1 mag in the H band for the 0.6% of sky not meeting the sensitivity requirement while meeting or surpassing the sensitivity requirement in the other two bands.

4. DATA PROCESSING

4.1. *Overview*

An automated software pipeline, the 2MASS Production Pipeline System (2MAPPS; Fig. 12), ingested a night's raw digital survey and calibration data from one observatory and output astrometrically and photometrically calibrated "Atlas Images" and tables of extracted source characteristics. Each 6° survey and 1° calibration scan was processed individually. 2MAPPS produced an extensive web-based quality verification report for each night's data that enabled monitoring of telescope and camera performance and assessment of the data's quality.

The entire 2MASS data set was processed twice. The first, preliminary processing was conducted while observations were ongoing and used a version of 2MAPPS that evolved continuously in response to instrumental changes and improving understanding of hardware and software system performance and calibration. This preliminary processing supported planning and telescope operations, as well as the generation of early data sets for public release.[19] Following the completion of telescope operations the entire data set was reprocessed with the ultimate version of the 2MAPPS pipeline. This final version of 2MAPPS incorporated the best knowledge of calibration, sky conditions, and system performance accumulated over the life of the survey. The 2MASS All-Sky Data Release Image Atlas and Catalogs are drawn from this final processing and replace any "Incremental Release" data products generated with earlier versions of the pipeline.

4.2. *Image Calibration*

Processing began with instrumental calibration of the raw image data. Each of the 1.3 s and 51 ms exposure raw image frames in a scan were corrected for instrumental signatures by subtracting a dark frame, dividing by a responsivity image (flat-field), and subtracting a sky-illumination correction image. The sky-illumination correction was a trimmed average of 42 consecutive frames representing a best estimate of the sky image in that portion of a scan with stars removed. Dark frames and flat-field sequences (from the evening or morning twilight sky) were acquired on a nightly basis when possible. During operations dark and flat-field frames were constructed from a running median of five nights of data. Study of these images indicated that the dark frames and the flat-fields were stable for long periods of time. Sixteen time periods, punctuated by significant events (summer shutdown, electronics adjustments, and one array change), were identified for the northern facility and four for the southern facility. For final processing a single flat-field and a single dark frame, assembled from the median of all of the available frames from a given time period, served as the calibration images for each period.

4.3. *Atlas Image Construction*

The overlapping calibrated individual 1.3 s frames were spatially registered using stars appearing in the overlap region between

[17] See http://www.journals.uchicago.edu/AJ/journal/issues/v120n6/200335/datafile3.txt.

[18] See http://www.ipac.caltech.edu/2mass/releases/allsky/doc/sec6_4b.html.

[19] The 2MASS First and Second Incremental Data Releases covered 6% and 47% of the sky, respectively.

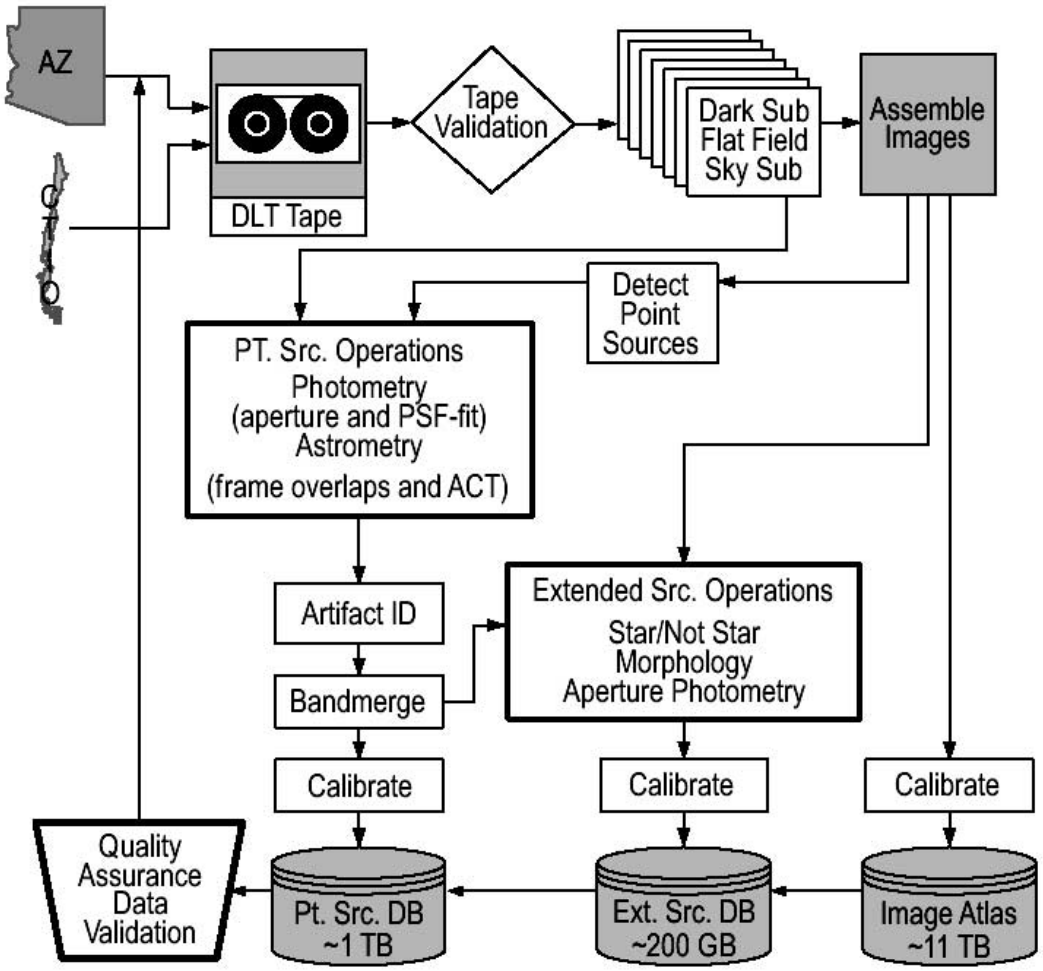

FIG. 12.—2MAPPS flowchart.

successive frames and combined to create Atlas Images that had a net exposure time of 7.8 s pixel^{-1}. Tycho-2 stars appearing along each scan tied the scan coordinate system onto the J2000.0 reference system and controlled the accumulation of random walk position error from frame to frame. Before frame combination, all J, H, and K_s frames were resampled on the same 1.″00 pixel^{-1} coordinate grid using a flux-preserving interpolation kernel. Detector pixels that had poor responsivity, were excessively noisy, or were affected by transient effects, such as meteor trails, satellite tracks, or cosmic rays, were masked off in the frames prior to the interpolation procedure. The registered and interpolated frames were averaged together in a continuous 6° strip. The output Atlas Images were written to FITS standard images in 512×1024 pixel (1.″00 pixel^{-1}) format with a 54 pixel overlap in the declination (long) direction for convenience. Most pixels of the Atlas Images represent the average of six 1.3 s frames. Because some pixels on the individual frames were masked and because there was some margin in the frame overlap, a pixel in the Atlas Images may occasionally represent the average of zero to seven frames. Each Atlas Image has a corresponding "coverage map" that represents, pixel by pixel, the number of samples contributing to each 1″ pixel.

4.4. *Point-Source Detection and Photometry*

The 2MAPPS point-source subsystem identified candidate point sources on the Atlas Images and then extracted flux estimates from the 1.3 s and 51 ms frames using both apertures of various sizes and profile-fit algorithms. In addition to fluxes, these algorithms reported a variety of diagnostic statistics and flags. The pipeline output populated a "working" database that contained every source extraction from every potentially photometric scan of a survey tile. The 2MASS Explanatory Supplement (Cutri et al. 2003) provides substantial detail on the source extraction algorithms and characteristics of the resulting data sets. The sections that follow (§§ 4.4.1–4.4.4) only highlight the most salient features of point-source extraction. Users of 2MASS data should regard the Explanatory Supplement as the only sufficient guide to productive scientific use of the 2MASS data sets.

4.4.1. *Profile-Fit Photometry*

In addition to reporting fluxes obtained via different extraction algorithms, the point-source subsystem populated a "default" magnitude column by selecting the result most likely to produce reliable photometry for a given source. The "default" magnitude for most unsaturated sources derives from a PSF profile-fitting algorithm. This algorithm provided the best accuracy for point sources with S/N $\lesssim$ 30 and in crowded regions. Sources were first detected on the Atlas Images (§ 4.3) prior to the extraction of profile-fit fluxes. Each Atlas Image was spatially filtered using a zero-sum 4″ FWHM Gaussian. Detections were identified as local intensity maxima that exceeded 3 times the estimated point-source noise level in the image. This low threshold ensured a high level of completeness in source extraction at the expense of

triggering the detection of many false sources that were filtered from the released data during final catalog generation. In source-confused regions the noise estimator produced a result consistent with the confusion noise. As a result, the detection threshold scaled naturally to higher fluxes in response to increasing source density.

For each source detection on an Atlas Image a PSF template indexed to the average Atlas Image FWHM was fit simultaneously to the source data from the six (and sometimes seven) individual 1.3 s frames covering the source. The sky background was estimated in an annular region with inner radius of 14″ and outer radius of 20″. The fit yielded an optimized position, flux, uncertainty, and χ^2 goodness of fit. Detections that fell within 5″ of each other were fit simultaneously. The uncertainties in the profile-fit photometry were based on the a posteriori covariance of the estimated fluxes and positions, taking explicit account of the PSF shape, using a measurement-noise model that included the effects of read noise, Poisson noise, and PSF error. Analysis of the rms statistics of repeated observations showed that for $S/N > 10$ sources the profile-fit algorithm overestimated the actual uncertainty. A magnitude-dependent correction was applied to the profile-fit uncertainties to make them consistent with the empirical uncertainties from repeated observations.

4.4.2. *Aperture Photometry*

In the absence of confusion, aperture photometry provided better accuracy for brighter sources ($K_s < 13$) than profile-fit photometry, since small deviations between the PSF templates and the true source profiles dominated the PSF-fit uncertainties. The pipeline extracted both aperture and PSF-fit measurements for each source when possible. Aperture measurements of each source detected on an Atlas Image used data from the individual 1.3 s frames. On each frame fluxes were measured in a series of circular apertures with radii from 3″ to 14″ on intervals of 1″. Sky brightness was estimated in an annulus with inner and outer radii of 14″ and 20″. The source flux in each aperture was the unweighted average of the fluxes measured on each frame. The aperture photometry uncertainty was the rms of these individual frame measurements.

The Point Source Catalog "standard aperture" magnitude was measured in a 4″ radius aperture.[20] The PSF of the 2MASS optical system was broad enough that between 2% and 15% of the total flux from a point source fell outside this aperture, depending on the atmospheric seeing conditions. A curve-of-growth correction was applied to the standard aperture measurements to compensate for this loss. With this correction applied the standard aperture measurement reflects the flux from an "infinite" size aperture that captures all of the light from the star image.

Magnitudes and uncertainties reported for sources that were saturated on the 1.3 s exposures were the average and rms of the aperture photometry measurements from the individual 51 ms exposure frames. Detections that contained one or more saturated pixels even on the 51 ms frames were estimated by fitting the nonsaturated part of their azimuthally averaged radial brightness profiles to one-dimensional analytic templates.

4.4.3. *Total Flux Uncertainty*

In addition to the default extraction uncertainty for each point source, the Point Source Catalog includes a column that reports a combined uncertainty that includes zero-point uncertainty, flat-field uncertainty, and, for sources saturated in the 1.3 s exposures, uncertainty in the normalization of the saturated photometry.[21] The largest of these additional uncertainty terms, which were combined in quadrature with the default source extraction uncertainty, was 0.012 mag. Thus, for most sources, the combined uncertainty is only slightly larger than the source extraction uncertainty.

4.4.4. *Band-Merging*

Although point-source detection and photometry was conducted independently for the J, H and K_s detections in each scan, the catalog contains a single entry for each source. The individual band detections were positionally "merged" into single source entries using a nearest-neighbor algorithm with logic to break merging conflicts and chains. No information other than positional data guided the merging algorithm. The final position quoted for each point source was derived from the flux-variance-weighted average of the position from each band detection.

4.5. *Extended Source Identification and Characterization*

The 2MASS Extended Source Catalog contains sources that are extended with respect to the instantaneous PSF, such as galaxies and Galactic nebulae. The 2MASS Explanatory Supplement, as well as Jarrett et al. (2000), describes the extended source component of the 2MASS pipeline in detail. Briefly, point/extended-source discrimination was conducted for each band-merged point-source detection by comparing a variety of radial shape, surface brightness, image moments, and symmetry parameters with characteristic stellar parameters using an oblique decision tree classifier. The classification tests included filters to exclude double and triple stars, which were one of the main contaminants in high source density regions. Stellar parameters were measured empirically as a function of time in each scan to compensate for variations in the atmospheric seeing using the aggregate properties of band-merged point-source extractions.

Once identified, extended sources were then extracted directly from the Atlas Images. Photometry was performed in a series of fixed circular apertures (5″–70″), circular and elliptical apertures defined by the source's J and K_s 20 and 21 mag arcsec^{-2} and Kron isophotes, and multiple apertures yielding extrapolated "total" magnitudes. Elliptical fits were made to the isophotal contours, yielding basic source shape parameters such as semimajor axes, axial ratios, and position angles. Background compensation for the extended source photometry was made by fitting and subtracting a low-order two-dimensional polynomial to the entire Atlas Image.

The extended source processing algorithm was not designed to extract the parameters for the largest galaxies on the sky. Although not a primary objective of 2MASS, high-quality infrared fluxes and spatial parameters for galaxies larger than 120″ in size have been reconstructed and delivered in the 2MASS Large Galaxy Atlas (Jarrett et al. 2003), which is included in the Extended Source Catalog.

4.6. *Position Reconstruction*

Source positions were reconstructed in the International Celestial Reference System (ICRS) via the Tycho-2 Reference Catalog (Hög et al. 2000). Position reconstruction involved three

[20] The standard aperture measurements appear in Point Source Catalog columns *j,h,k_m_stdap*.

[21] Catalog columns *j,h,k_cmsig* denote the default source extraction uncertainty, while columns *j,h,k_msigcom* contain the combined uncertainty.

steps. First, point-source extractions in overlapping frames were used to determine the relative frame offsets. Second, astrometric reference stars were identified among the extractions, and their scan positions were used to tie together the three bands in both the short 51 ms and standard 1.3 s images simultaneously. Doing so constrained the random walk errors in the frame offsets along a scan and mapped the scan reference frame onto the astrometric grid. During preliminary 2MASS data processing, source positions were reconstructed using the Astrographic Catalog–Tycho-1 (ACT) Reference Catalog because Tycho-2 was not yet available. Tycho-2 was used as the primary astrometric reference in the final data processing. The third position reconstruction step, performed only in final data processing, used the position differences of sources appearing in the overlapping regions of adjacent scans to constrain astrometric solutions across scan boundaries. Doing so improved the uniformity of astrometric solutions on larger spatial scales, particularly for scans with relatively few or poorly distributed Tycho-2 reference stars. Astrometric solutions for each scan were incorporated into the World Coordinate System information in each 2MASS Atlas Image.

The 2MASS position uncertainties incorporate contributions from four components. Uncertainties associated with source extraction were computed by fitting a template to the stack of overlapping 1.3 s exposures of the source from a single band's scan data. The dispersion about the fit determined the extraction position uncertainty. This single-band position measurement was transformed to a multiband coordinate system that incorporated information from each of the three bands. Uncertainties in registration of single-band coordinates to the multiband coordinate system were determined empirically from the dispersion in position discrepancy of astrometric standard stars across the different single-band systems. In determining a single position and uncertainty for a band-merged source, the two uncertainties above were root-sum-squared for a given source to arrive at the uncertainty in the multiband coordinate. When band detections were merged, their independent positions were combined via inverse-variance weighting to compute the refined position, and the refined uncertainties were computed accordingly. Ultimately, positions were transformed to the celestial coordinate system. Uncertainties in position on the celestial sphere were determined empirically from position differences of sources observed in the scan overlap regions and from the position residuals of Tycho-2 astrometric reference stars as a function of position along the scan. The resulting uncertainties were then added in quadrature to those above.

4.7. *Artifact Identification*

Likely spurious extractions triggered by artifacts of bright stars were automatically identified in the point- and extended-source lists using geometric and brightness-based algorithms. Possible artifacts were selected by searching template areas around bright stars that were known to be affected by scattered light, diffraction spikes, dichroic glints, latent images, and electronic cross-talk banding. The extent of the affected area was a function of the star's brightness and the scanning step size. Discrimination between spurious detections and real sources was attempted via the assignment of a probability of contamination. Probable spurious extractions were excluded from the release catalogs. The list of identified artifacts was maintained, however, in order to create image overlays for the Atlas Images so that users could readily distinguish likely artifacts from real sources in the images.

During the final reprocessing of the data, meteor trails, which typically appear on only one of the six frames covering a given sky location, were removed prior to the construction of the Atlas Images. This procedure eliminated virtually all of the spurious source extractions along the trails and cleaned the trails from the Atlas Images.

Artifact identification, although efficient, was not perfect. The survey's requirements allow $<0.05\%$ of the sources with $S/N > 10$ in any one band to be artifacts. The Point Source Catalog contains 321 million sources with $S/N > 10$, and the requirement allows for more than 100,000 unidentified artifacts in this subset. Section 5.2.8 discusses the characterization of the achieved reliability of the Point Source Catalog.

4.8. *Quality Assurance*

Verification and validation of pipeline data quality used an automated software system that generated a set of HTML reports summarizing characteristics such as telescope tracking and scanning stability, detector noise levels, nightly photometric stability from the calibration solutions and the photometric consistency of sources extracted from overlapping regions of scans, atmospheric seeing and background levels, astrometric solution performance, and the incidence of transient events such as aircraft passages, bugs on the camera windows, etc. Each scan was assigned a quality score depending on these quantitative performance criteria. Quality assurance scientists reviewed the automated reports for each night, confirming or adjusting the resulting quality scoring as necessary. During nightly operations the observatory scheduling software incorporated these quality scores to establish the nightly priority for tile observation. For final processing, the quality assurance scoring drove selection of scans for inclusion in the 2MASS All-Sky Data Release products.

4.9. *Final Product Generation*

The final data processing generated "working" source databases that contained 1,314,981,867 and 2,590,500 extractions of point and extended sources, respectively, from 70,712 scans of survey tiles. The number of sources in the working databases was substantially larger than the number of sources in the final catalogs because the working databases contained (1) multiple detections of sources scanned more than once because they fell in tile overlap regions or because they were in tiles that were reobserved and (2) extractions of faint, often unreliable, sources resulting from the low detection thresholds used to ensure completeness. The data release requirements dictated that the final catalogs meet a higher standard of uniformity and reliability than the contents of the working databases. The final Point and Extended Source Catalogs included a subset of the contents of the working databases based on the following procedures:

1. Select the best scan of any multiply observed tile, based on net photometric sensitivity.
2. Select a single apparition of any multiply detected source falling in a tile overlap region using a purely geometric algorithm that chose the apparition falling farthest from a tile edge. Basing this choice only on source position minimized spatial bias in the catalogs from the tile overlap regions.
3. Remove sources with high probability of being an artifact.
4. Select point sources with $S/N > 7$ in at least one band or $S/N > 5$ in at least one band but detected in all three bands.
5. Select extended sources with $S/N > 7$ in at least one band.

Additional diagnostic/summary information was generated for each source selected into this catalog subset. These post-processing "value-added" data columns included such quantities as the separation and position angle of a given source from

its nearest neighbor in the catalog. Another Point Source Catalog column combined S/N, χ^2, detection repeatability, scan background noise, and detection upper limits band by band into a single shorthand three-character photometric quality flag.[22]

5. ACHIEVED PERFORMANCE

5.1. *Data Product Summary*

Final product generation created a Point Source Catalog containing 470,992,970 sources and an Extended Source Catalog of 1,647,599 sources, along with 4,121,439 FITS images from the 59,731 unique scans from which these sources were selected. These products along with several ancillary tables constitute the 2MASS All-Sky Data Release[23] made available to the public in 2003 March. Figure 13 graphically illustrates the contents of the primary catalogs with all-sky projections reconstructed from the entries in the Point and Extended Source Catalogs.

5.2. *Point-Source Performance*

The 2MASS Science Team carried out a number of analyses to validate and characterize the All-Sky catalogs. These analyses operated on the catalogs themselves, as well as on data sets such as the calibration data, which were processed in a manner identical to the primary data. The calibration data, in particular, contained thousands of repeated apparitions of sources. Statistics of these repeated observations formed the basis for empirical estimates of uncertainties, completeness, and reliability. Table 2 summarizes the primary characteristics of the 2MASS Point Source Catalog determined by these analyses.

5.2.1. *Sky Coverage*

2MASS imaged 99.998% of the celestial sphere in all three bands, missing 0.64 deg^2 owing to 50 mispointed tiles that left narrow uncovered gaps relative to neighboring tiles. Since source extraction required that a point source be $>10''$ from a tile edge, the uncovered regions of the Point Source Catalog amount to 1.152 deg^2.[24] The area lost to these gaps is small compared with the area lost by the exclusion of sources in a magnitude-dependent radius around bright stars. These avoidance areas, invoked to minimize the incorporation of false detections due to artifacts, reduce the catalog's sky coverage to 99.5%.

5.2.2. *Dynamic Range*

2MASS photometry has a dynamic range of >20 mag owing to the source extraction software's ability to address different exposure regimes. Unsaturated sources in the nominal 1.3 s exposures (mag ~8–17) and in the 51 ms integrations created by the first readout of the array following reset (mag ~4–8) were extracted using aperture and/or profile-fit photometry techniques. Flux estimates for sources that saturated the 51 ms exposures were provided by template fitting to the unsaturated scattered light in the wings of the saturated star image (mag ≤ 4).[25] The brightest K_s-band source extracted by the pipeline was α Orionis at $K_s = -4.4$ mag, while the faintest common K_s extractions appearing in the Point Source Catalog have $K_s \sim 16.2$ mag. Figure 14 presents source counts at the north Galactic pole from the 2MASS Point Source Catalog in all three bands spanning the full dynamic range.

5.2.3. *Photometric Sensitivity*

Figure 15 shows the rms flux uncertainty versus magnitude for each star in one set of six consecutive observations of a 2MASS calibration tile. This statistic establishes the S/N = 10 limiting magnitudes for that set of observations and thus for the conditions of seeing and background that prevailed at the time of observation. Evaluation of such statistics for the ensemble of calibration scan data established a relationship for the S/N = 10 limiting fluxes of any given survey scan as a function of the background and seeing. Survey scans that fell below the sensitivity requirements were scheduled for reobservation.

The histograms in Figure 16 document the S/N = 10 sensitivity for every scan used in the 2MASS All-Sky Data Release as established by the scan's background and seeing. Although the 2MASS sensitivity specification was $J = 15.8$, $H = 15.1$, and $K_s = 14.3$ at S/N = 10, Figure 16 demonstrates that the bulk of the data are substantially more sensitive than these goals, particularly in the J band. Because sensitivity varied from tile to tile, the source counts in the raw Point Source Catalog are spatially nonuniform, with structure that reflects the tile pattern. Since the source counts are >99% complete at the S/N = 10 limits in the absence of confusion, the catalog becomes uniform at high Galactic latitude at magnitudes brighter than the S/N = 10 specifications above. At low Galactic latitude source confusion raises the flux level at which the completeness requirement is met (§ 5.2.9).

5.2.4. *Photometric Accuracy*

All except two of the 59,731 survey tiles were observed under photometric conditions according to quality assurance measures. Thin clouds were detected in small portions of the scans of two tiles during final processing, and sources in these regions were assigned appropriately large photometric uncertainties and correspondingly poor photometric quality flags.

The statistics of repeated observations served to validate the flux uncertainties assigned to individual sources by the extraction algorithms (Fig. 15). As discussed in § 4.4.1, the bulk of the default photometry in the Point Source Catalog arises from the profile-fit algorithm. This algorithm consistently overestimated the true flux uncertainty, and the extracted uncertainties were scaled to match the empirical uncertainties from the repeated observations. Figure 17 illustrates the locus of flux uncertainty for K_s-band sources across the entire dynamic range of 2MASS. At faint magnitudes ($K_s > 13$) uncertainties rise due to the dominance of background noise. For $8.5 < K_s < 13$ default uncertainties are consistently in the range 0.02–0.03 mag. This limiting profile-fit uncertainty is attributable to PSF mismatch in the profile-fit algorithm, driven by undersampling due to the coarse $2''.0$ pixel size.

Fluxes for stars with $4 < K_s < 8.5$ were measured with aperture photometry in the six or seven independent 51 ms exposures since their images saturated the 1.3 s frames. Since aperture photometry provides a more consistent flux estimate than profile-fit photometry for brighter stars, these stars have mean uncertainties (*light blue points*) that are smaller than the profile-fit extraction uncertainties. Stars whose images were saturated even on the 51 ms exposures ($K_s < 4$; *dark blue points*) have much larger

[22] This photometric quality flag, *ph_qual*, readily identifies sources with S/N > 10 in one or more bands via the appearance of one or more "A"s in the entry. The survey's requirements in Table 1 for completeness, reliability, and uniformity apply to the 321 million sources in the Point Source Catalog meeting this condition.

[23] See http://www.ipac.caltech.edu/2mass/releases/allsky/.

[24] The locations of these coverage gaps are documented at http://www.ipac.caltech.edu/2mass/releases/allsky/doc/sec3_2c.html.

[25] The Point Source Catalog *rd_flg* column reports, band by band, the photometry method used to populate the default magnitude column.

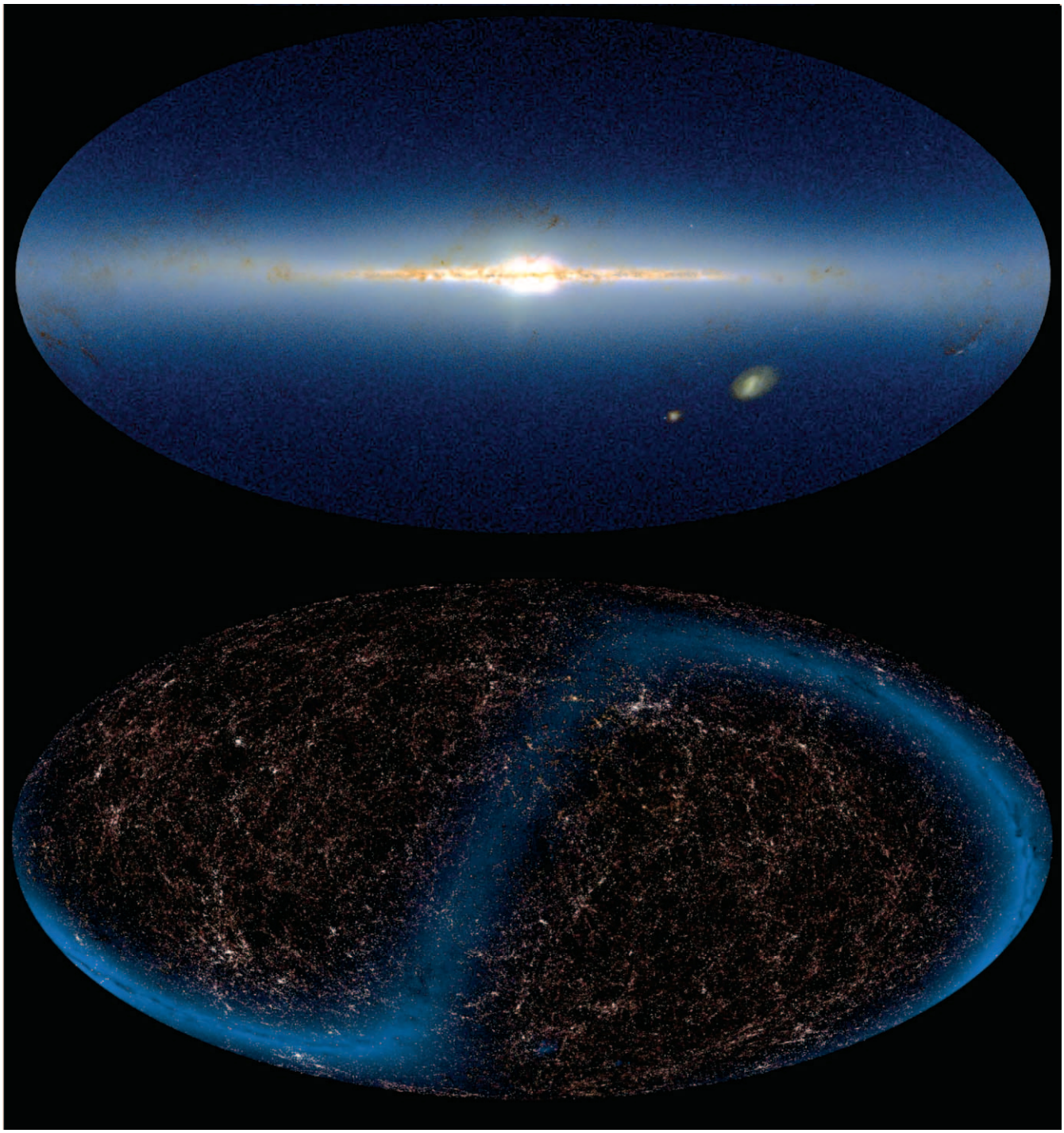

FIG. 13.—Full-sky distribution of point (*top*) and extended (*bottom*) sources. Point sources are presented in Galactic coordinates centered on $b = 0^\circ$ and $l = 0^\circ$. The extended source map is presented in equatorial coordinates and centered at $\alpha = 180^\circ$ and $\delta = 0^\circ$. The faint blue band in the extended source map traces the Galactic plane as represented by the Point Source Catalog. Intensity is proportional to source density. The images are a color composite of source density in the J (*blue*), H (*green*), and K_s (*red*) bands.

TABLE 2

2MASS POINT SOURCE CATALOG PERFORMANCE

Category	Performance
Dynamic range	>20 mag (−4 through 16 mag at K_s)
Sensitivity in unconfused regions	100% of coverage better than S/N = 10 at $J = 15.9$, $H = 15.0$, and $K_s = 14.3$ mag; 50% of coverage better than S/N = 10 at 16.4, 15.5, and 14.8 mag, respectively; most sensitive individual tile S/N = 10 at 16.8, 16.0, and 15.3 mag
Photometric precision	<0.03 mag (1 σ) for bright (<13.0 mag) stars
Photometric uniformity	<2% photometric bias for any point on the sky
Astrometric accuracy	≲100 mas (1 σ) absolute relative to the *Hipparcos* reference frame for $K_s < 14$
Completeness	>99% for sources with S/N > 10 in any one band
Reliability	>99.95% for sources with S/N > 10 in any one band

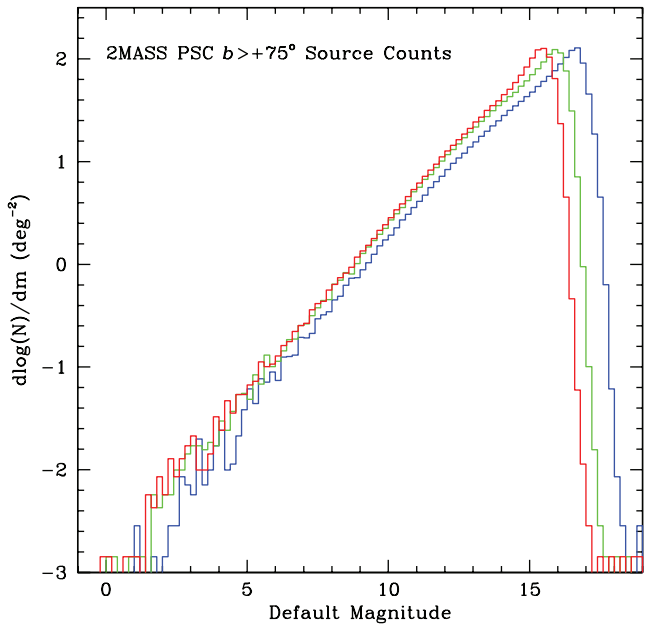

FIG. 14.—2MASS Point Source Catalog source counts (per 0.2 mag bin) for several hundred square degrees near the north Galactic pole. Blue, green, and red histograms represent J, H, and K_s counts, respectively.

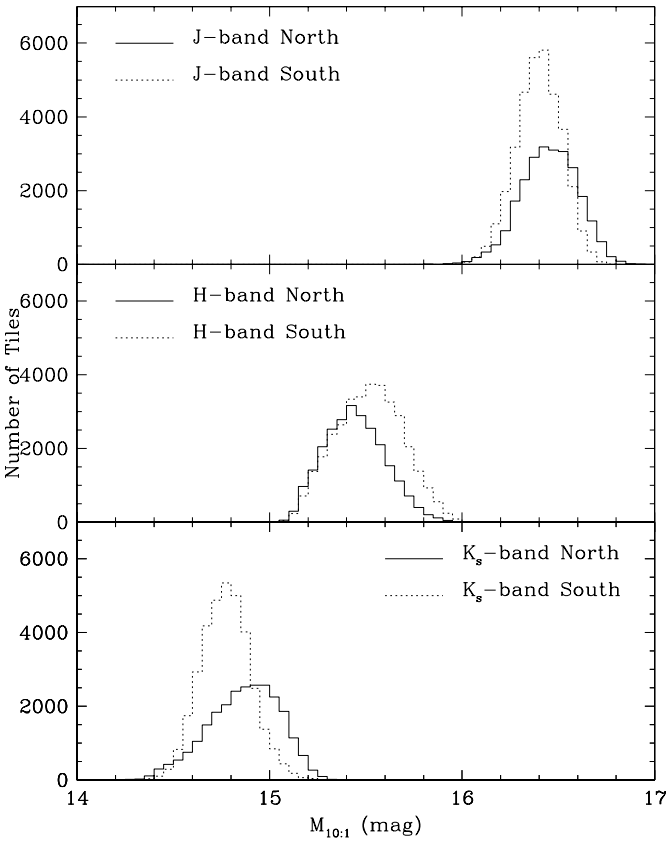

FIG. 16.—Histograms of the distribution of the S/N = 10 sensitivity level divided by hemisphere for each of the 59,731 scans that comprise the 2MASS catalogs.

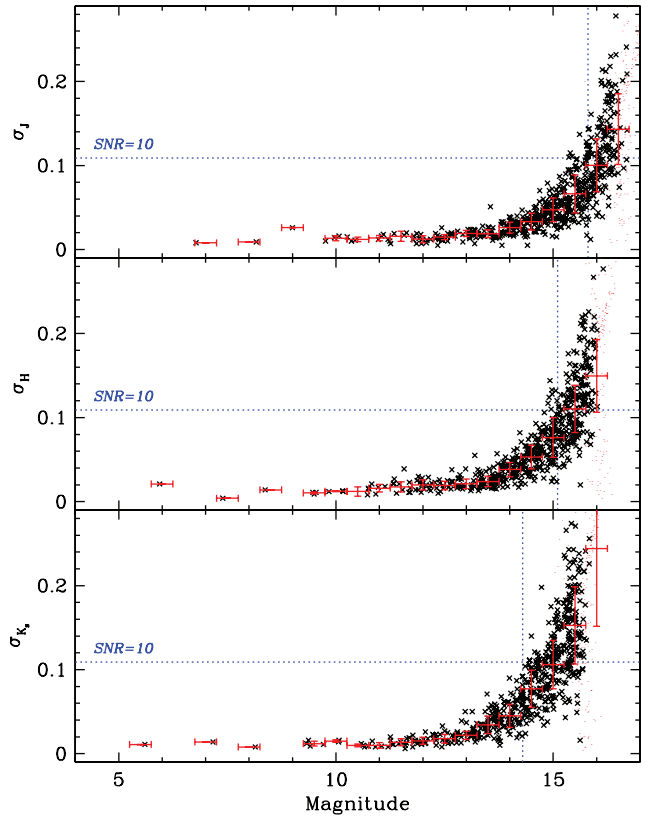

FIG. 15.—Sensitivity vs. magnitude distributions obtained from the rms of the six independently derived magnitudes of each star appearing in one set of six calibration scans. The black crosses are the measurements of individual stars; red bars are the trimmed average rms values for all stars in 0.5 mag wide bins. The horizontal blue lines in each panel indicate the S/N = 10 levels, and the vertical blue lines show the survey's S/N = 10 requirements.

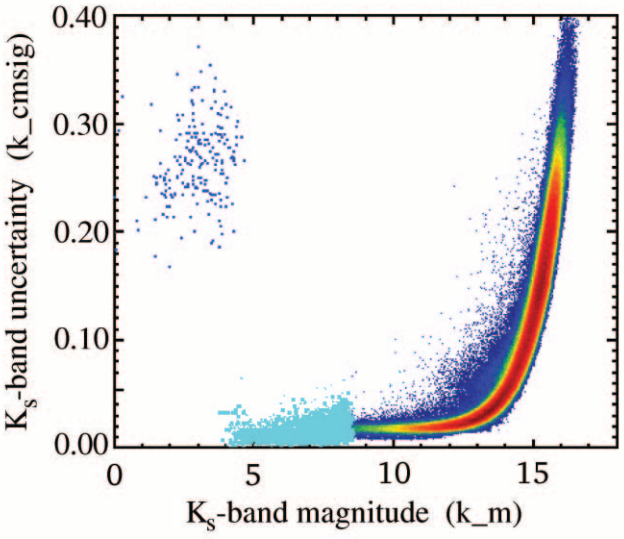

FIG. 17.—Reported default uncertainty (*k_cmsig*) as a function of magnitude for the K_s band. Faintward of $K_s \sim 9$ a Hess diagram represents the density of occurrence of different values of *k_cmsig* in the Point Source Catalog. For $4 < K_s < 9$, light blue points represent the uncertainties for individual sources that were saturated in the 1.3 s standard exposure time but were unsaturated in the 51 ms exposures. The dark blue individual points for $K_s < 4$ represent the uncertainties for sources that saturated the 51 ms exposures whose fluxes were estimated from fits to the unsaturated wings of the stellar profile.

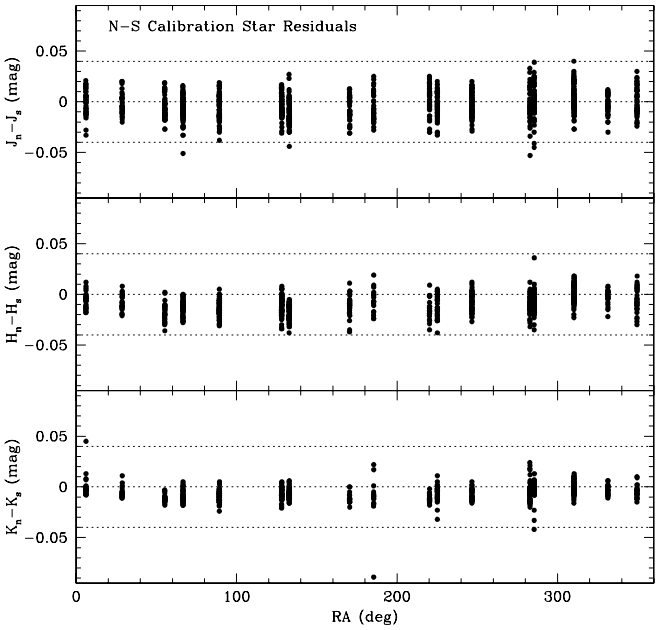

FIG. 18.—Difference in magnitude assigned by the global calibration algorithm vs. right ascension for standards derived independently from northern and southern observatory data. Each cluster of points represents the magnitude differences for stars in a single calibration tile. The calibration tiles in common between hemispheres lie largely along the celestial equator.

uncertainties because fluxes were estimated from a fit to the wings of the saturated stellar profile. The magnitude boundaries between these regimes vary by a few tenths of a magnitude depending on the wavelength band and seeing and background conditions.

5.2.5. *Photometric Uniformity*

Large-scale drifts in the 2MASS photometric system were minimized using the global photometric calibration procedure of Nikolaev et al. (2000) described in § 3.4. Photometric solutions were established independently for each hemisphere's data. Calibration stars shared by both hemispheres exhibit <2% bias in their independently derived fluxes (Fig. 18).

The colors of main-sequence stars provide another test of photometric uniformity. Each night has an independent calibration solution. If these solutions are significantly dispersed or biased, a global compilation of 2MASS photometry, spanning many nights of observation, will be substantially broadened and/or offset from a single night's results. Figure 19 confirms that the color locus for a single night's observations is largely indistinguishable from a random sampling of thousands of square degrees of sky drawn from the opposite hemisphere.

5.2.6. *Astrometric Accuracy and Uniformity*

Comparison of the 2MASS point-source positions with the Tycho-2 catalog (Hög et al. 2000) and the USNO CCD Astrograph Catalog (UCAC; Zacharias et al. 2000) demonstrate that 2MASS positions are consistent with the ICRS with a net offset no larger than 15 mas. Position residuals of individual sources validate a typical positional uncertainty for $K_s < 14$ sources of $\lesssim$100 mas (rms). This positional uncertainty is consistent with the internal scatter in repeated observations of sources in overlapping scan regions (Fig. 20).

5.2.7. *Completeness*

The thousands of repeated calibration observations enabled an assessment of completeness as a function of magnitude from the number of times a source of a given magnitude was detected relative to the number of opportunities. Figure 21 shows that this empirical measure of completeness declines steeply faintward of the S/N = 10 sensitivity threshold. Since this S/N = 10 threshold depends on the background and seeing conditions that prevailed at the time of observation, each scan will have a different completeness threshold. 2MASS provides an ancillary Scan Information Table that includes columns detailing the estimated

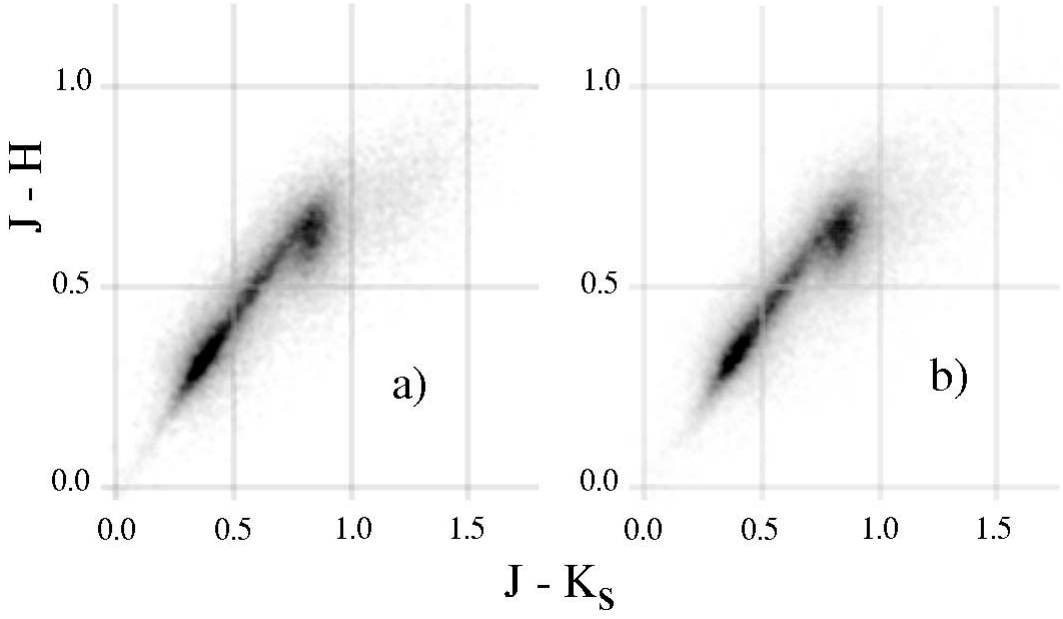

FIG. 19.—Hess diagrams of color-color distributions obtained for two different regions of the sky: (*a*) a "local" region of northern hemisphere data from the night of 1999 February 28 UT (about 30 deg^2); (*b*) sources randomly selected from Galactic latitudes below $b = -40°$ and between declinations $-40°$ and $-70°$ in the southern hemisphere, thus including data from hundreds of nights. The similarity of the distributions confirms the consistency of the nightly calibration solutions. The differences in the faint distribution of sources for $J - K_s > 1.0$ reflects actual differences in extragalactic populations in the "local" vs. "global" samples.

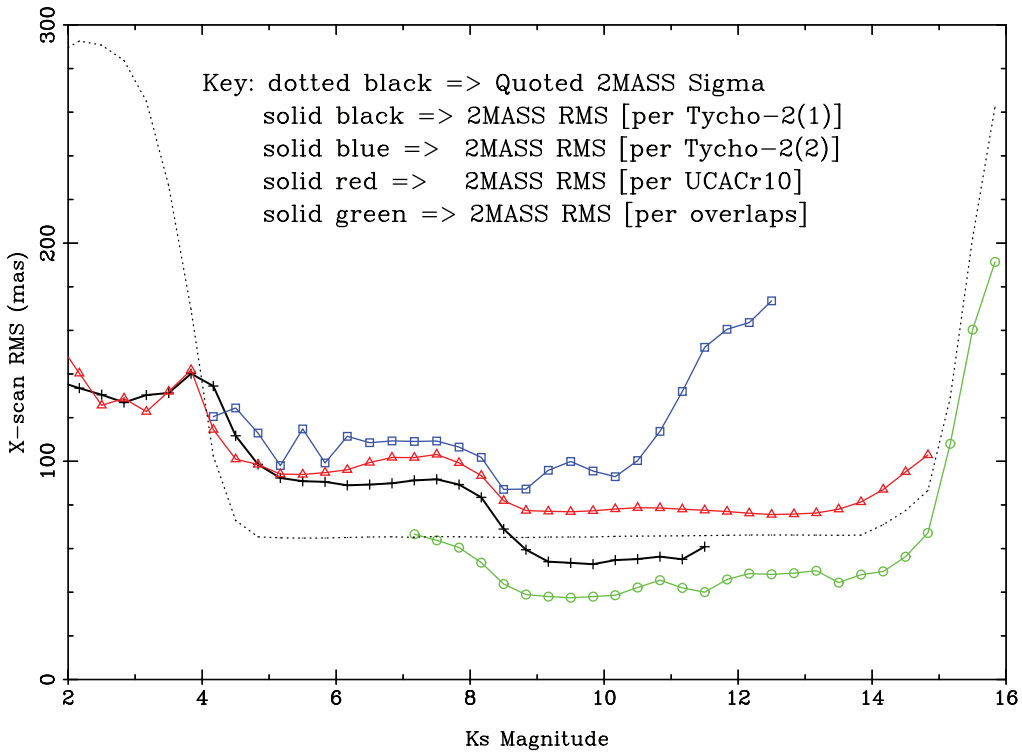

FIG. 20.—Astrometric comparison between 2MASS and other catalogs as a function of 2MASS K_s magnitude. The solid black curve indicates rms position differences in the cross-scan (right ascension) direction between 2MASS and the subset of Tycho-2 stars that appeared in Tycho-1 [Tycho-2(1)], while the blue curve is for sources appearing in Tycho-2 [Tycho-2(2)]. This latter subset did not appear in Tycho-1 and thus includes fainter stars with poorer position estimates. Position residuals with UCAC are indicated in red. The green line represents internal 2MASS position differences between adjacent tiles. Analysis of the component of position error along the scan direction yields similar results.

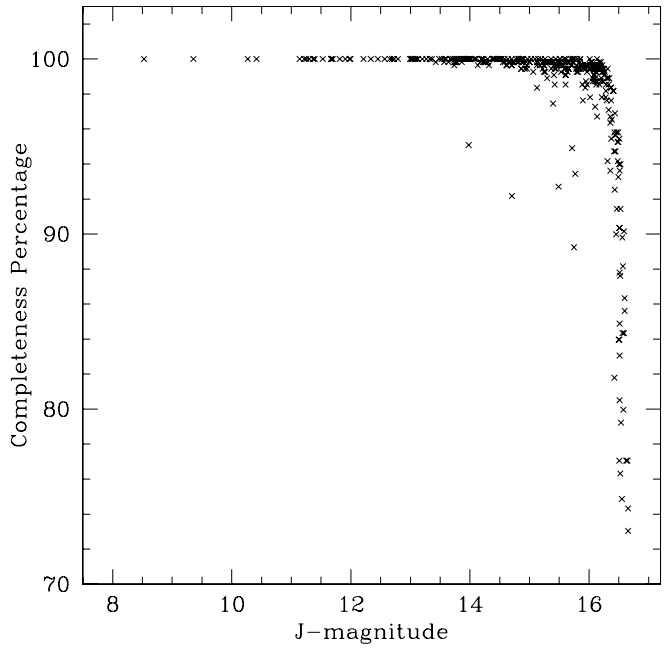

FIG. 21.—Completeness vs. magnitude for a set of 549 observations of calibration field 90161 where the J-band S/N = 10 sensitivity was near the median value for all scans contributing to the Point Source Catalog, $J = 16.4$. Each point represents the detection percentage in the 549 trials for a given star. Visual examination of star images corresponding to points that lie well away from the overall locus reveals that these are close pairs at the threshold of the resolution of the survey and sources near bright stars.

sensitivity at the time of observation for each tile to enable robust statistical analysis of the whole sky accounting for the varying completeness threshold. Since virtually all of the 2MASS scans have S/N = 10 sensitivity better than the requirements of 15.8, 15.1, and 14.3 mag for J, H, and K_s, respectively (Fig. 16), the Point Source Catalog is >99% complete above these limits for nearly the entire unconfused sky.

5.2.8. *Reliability*

A reliable source is one that can be detected repeatedly, within the constraints of possible proper motion or flux variability. In practice, reliability represents the ratio of the number of "real" astronomical sources to the total number of sources in the data set. The survey's requirements dictated that Point Source Catalog reliability should exceed 99.95% for sources detected at or above the S/N = 10 threshold in any one band. The Point Source Catalog contains 321 million sources meeting this single-band S/N = 10 criterion. The 99.95% reliability requirement allows for 160,000 spurious extractions with S/N > 10 in one band in the Point Source Catalog.

The reliability of the Point Source Catalog was assessed via both external and internal comparisons. The sensitivity of the visible-wavelength SDSS exceeds that of 2MASS for the detection of all but the intrinsically reddest objects. Comparison with the SDSS Early Release Area yielded a reliability of 99.981% for the Point Source Catalog for sources with S/N > 10 in any one band. Internal tests for reliability used repeated observations of sources near the celestial poles, where the tiles converged and thus overlapped heavily. Fields with at least six independent observations yielded differential reliability in the 0.5 mag wide bins above the S/N = 10 limits of 15.8, 15.1, and

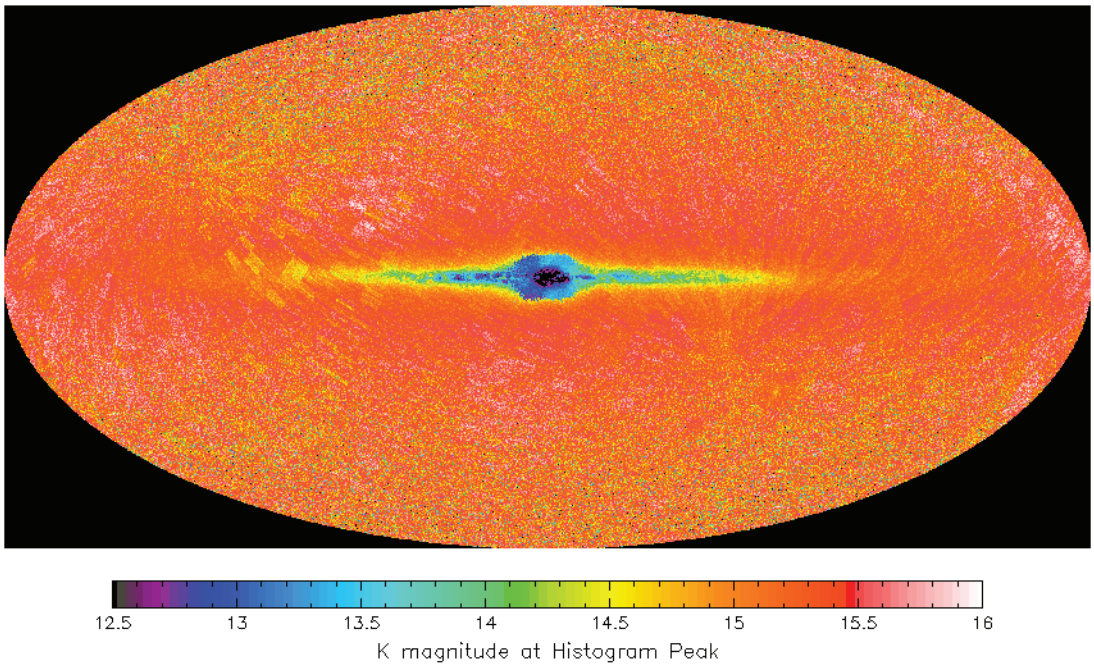

FIG. 22.—Full-sky projection illustrating the spatial distribution of source confusion in the K_s band. The color coding reflects the magnitude of the peak of the source counts vs. magnitude histogram for each direction in the sky. Although some overall variability in limiting magnitude arises from the variation in seeing and background level, confusion noise dominates the noise near the Galactic plane and thus raises the limiting flux for detection significantly.

14.3 mag at J, H, and K_s, respectively, of 99.98%, 99.98%, and 99.96%.

These tests revealed unreliable source extractions and thus general causes of unreliability within the catalogs. Sources detected in only one band had the greatest potential for being unreliable, particularly those detected only in the intermediate-wavelength H band. A limited number of unstable pixels created single-band unreliable sources. The worst of these bad pixels were identified, and their artifacts were removed from the catalogs. The surviving "hot pixel" sources are weakly distinguished from real sources, and attempts to remove them would have adversely affected completeness.

Bright stars created significant scattered light artifacts in their vicinity. Most of these were geometrically identified and removed from the catalogs. A small number of otherwise unidentifiable artifacts remain as unreliable sources. Other sources of unreliability include detections of sources triggered by satellite trails, meteoroids, and even insects. The majority of the resulting unreliable sources were removed from the catalog, and only a small residual contamination remains. Finally, minor planets with known ephemerides were identified and flagged in the Point Source Catalog (and cross-identified in a separate minor planet ancillary table). Unidentified minor planets contribute to unreliability, despite being real sources, since they do not adhere to the requirement of repeatable detection at the same position.

5.2.9. *Confusion*

The nominal 2MASS sensitivity limits apply to regions where the sky background dominated the noise. In regions of high stellar density such as dense clusters and the Galactic plane near the Galactic center, confusion from unresolved sources dominated the background Poisson noise. Source count versus magnitude histograms reveal the effects of confusion, since the confusion noise statistics dictate the limiting magnitude for completeness. Figure 22 shows the all-sky distribution of limiting magnitude for K_s-band source counts. The figure demonstrates that confusion restricts the sensitivity of 2MASS for only a small region of the inner Galactic plane at K_s band. Since interstellar extinction is at a minimum in the K_s band, the J and H bands are less affected by confusion. The primary areas of confusion are (1) longitudes $\pm 75^\circ$ from the Galactic center and latitudes $\pm 1^\circ$ from the Galactic plane and (2) within an approximately 5° radius of the Galactic center.

5.3. *Extended Sources*

Since the 2MASS millijansky flux limits favor the detection of Galactic stars over extragalactic sources (cf. Glazebrook et al. 1994), the 1.6 million object 2MASS All-Sky Extended Source Catalog, which itself is dominated by galaxies, contains only one source for every 300 counterparts in the Point Source Catalog. These 1.6 million extended sources adhere to similar high standards of uniformity, completeness, and reliability. Fixed-aperture measurements of repeated observations of extended sources demonstrate S/N = 10 sensitivity limits fainter than 15.0, 14.3, and 13.5 mag at J, H, and K_s band, respectively. The mean color difference of the high Galactic latitude extended source population is <0.01 mag between hemispheres, consistent with knowledge of the uniformity of calibration (§ 5.2.5). Completeness at the S/N = 10 flux limit cited above is >90% for sources more than 30° from the Galactic plane. This level of completeness is validated both through log (N) versus log (S) source counts and through comparison with external catalogs (Fig. 23). Extensive visual inspection of 2MASS extended sources and comparison with SDSS Early Data Release classifications yield an extended source reliability of >99% for Galactic latitudes more than 20° away from the Galactic plane. For the Extended Source Catalog, reliability refers to the correct identification of a catalog entry as representing a truly diffuse object as opposed to, for example, two or three merged star images. Jarrett et al. (2000) discuss, in detail, the performance of the extended source extraction pipeline and its effectiveness in

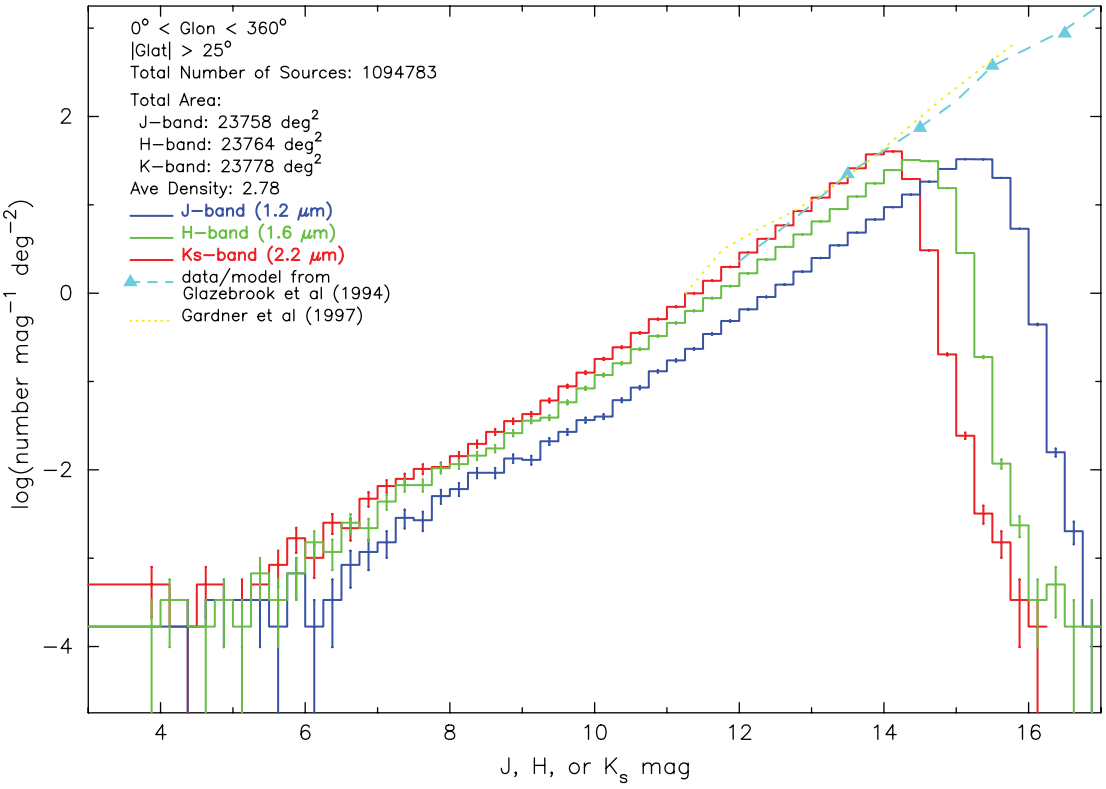

FIG. 23.—The J (*blue*), H (*green*), and K_s (*red*) source counts vs. magnitude for the Extended Source Catalog. The blue triangles and dashed line represent data from Glazebrook et al. (1994) for $K_s > 13.5$ with an extension to $K_s = 12$ using their no-evolution model. The yellow dotted line represents source counts from Gardner et al. (1997).

discriminating against false sources and separating stars from galaxies.

6. EXPLANATORY MATERIALS AND DATA DISTRIBUTION

All of the topics addressed in this paper are analyzed in depth in the 2MASS All-Sky Release Explanatory Supplement (Cutri et al. 2003). In addition to describing the details of the observation hardware, data processing, and the characteristics of the catalogs, this supplement provides substantial guidance in the astronomical use of the catalogs and describes potential pitfalls awaiting an uninformed user. The Explanatory Supplement is a "living" HTML document that is updated with new information as it becomes available.

Formal release of the 2MASS Point and Extended Source Catalogs and Ancillary Tables occurred in 2003 March via the distribution of five double-sided single-layer DVD-ROM disks containing 43 Gbytes of compressed ASCII bar-delimited tables formatted for direct loading into a computer database. This All-Sky Data Release supplants all previous "incremental" release data, replacing the preliminary source extractions and images from the incremental release products with ones that have been processed through the final version of the data pipeline. The All-Sky data have been made publicly available via the internet at the Infrared Science Archive (IRSA)[26] where they can be manipulated online through Structured Query Language (SQL) commands. The volume of the 2MASS All-Sky Image Atlas database (10 Tbytes uncompressed) prohibited an initial media release of Atlas Images. Instead, the IRSA site initially provided access to "quick-look" images stored with 20:1 lossy compression using the HCompress algorithm (White et al. 1992). Subsequently, mass storage has become available to serve these images without compression loss.

[26] See http://irsa.ipac.caltech.edu.

7. DEFINING CHARACTERISTICS

A large project can be characterized by a number of defining features and innovations. Even small decisions can have significant leverage on the overall success of a large enterprise. At the risk of repeating some of the discussion of 2MASS characteristics above, this section collects and summarizes a number of the factors contributing to the quality and uniformity of the 2MASS data products.

7.1. *Role of Prototyping*

The 2MASS project benefited from three years of prototyping of the survey's hardware and observational techniques. During this period data were acquired in the same freeze-frame scanning format as the survey itself, but with a camera containing a single NICMOS3 array (Beichman et al. 1998). Prototyping validated the efficacy and efficiency of the freeze-frame scanning technique, and the single-channel camera optical design was iterated during the prototyping campaign to become the basis for the final survey camera design. The prototyping exercise permitted initial development of the data processing pipeline in advance of the start of formal observations and, more importantly, validated assumptions regarding the end-to-end performance of the system. This knowledge of the likely sensitivity, completeness, and reliability during operations enabled the development of a robust set of testable requirements for success (outlined in Table 1) that, if met, would support the pursuit of the survey's primary science. These requirements remained unaltered and uncompromised throughout the survey and thus became a driving

factor in maintaining the quality and uniformity of the final data products.

7.2. *Telescope and Camera Features*

The 2MASS telescope and camera designs were straightforward implementations of existing technologies. This simplicity contributed substantially to the successful fabrication of the facilities and to their smooth operation, not to mention the timely completion of observations and the uniformity of the data products between hemispheres. The 2MASS cameras, for example, could have incorporated the then newly available 1024×1024 format arrays or could have multiplexed several NICMOS3 arrays per band. Doing so, however, could have added substantial risk to the project schedule and/or complicated day-to-day operations and data processing.

7.2.1. *Optical Design*

The 2MASS camera optical design itself was simple in that it was identical, in triplicate, to the successful and well-characterized prototype optical design. More importantly, this design produced uniform image shape and minimal distortion across the entire $8\farcm5$ field of view, simplifying the frame combination and profile-fit photometry algorithms. Incorporating dichroic mirrors into the optical design permitted simultaneous imaging of a field in all three colors, thus streamlining many aspects of the data pipeline and avoiding band-to-band systematics from variable seeing and telescope pointing.

7.2.2. *Focus Stability*

Invar focus spacers between the primary and secondary mirrors reduced the thermal variation in telescope focus by an order of magnitude compared with steel. The telescope control computer adjusted the secondary mirror focus as a function of telescope frame temperature to compensate for the residual focus variation attributable to the Invar. This active focus control eliminated the need for real-time focus feedback from the incoming images. After data tapes arrived at IPAC, analysis of the slight astigmatism introduced into the cameras by the dichroic mirrors permitted monitoring of any long-term accumulation of focus error. Seasonal adjustments of 10 μm in the secondary mirror zero position compensated the focus for the largest temperature swings.

7.2.3. *Freeze-Frame Scanning*

The 2MASS secondary mirror tilted to freeze the focal plane while the telescope scanned in declination, representing the first large-scale implementation of freeze-frame scanning in astronomy. This technique was extremely efficient. Frame-to-frame settling time was dominated by the inertial mass and resonant frequency of the secondary mirror rather than that of the entire telescope. Of the 1.455 s cycle time, only 51 ms was required for secondary mirror flyback and settling; during the remaining time the focal plane image was frozen in place and the array was integrating on sky. The regular exposure timing enforced substantial uniformity on the individual image frames, which in turn was one of the key factors that enabled the automated data pipeline to combine frames accurately and extract consistent results.

7.2.4. *Subpixel Sampling*

Freeze-frame scanning provided a natural means of recovering spatial information from the undersampled $2\farcs0$ per camera pixels. Because the telescope was scanning smoothly in the declination direction and because successive frames were offset $\sim 83''$, simple rotation of an array provided precise subpixel stepping in the direction perpendicular to the scan direction. Similarly, given the fixed frame-to-frame time interval, the telescope scan rate was adjusted so that a star would land with consistent subpixel offset from frame-to-frame in the direction along a scan. These two independent "substeps" were tuned to produce sampling that optimally recovered a smooth system PSF (Fig. 8). The data processing pipeline's quality assurance output monitored the subpixel stepping pattern for each scan.

7.2.5. *Hardware Redundancy and Modularity*

The northern and southern observatories, cameras, and data acquisition systems were nearly identical. Because of this similarity, construction of the northern facility prior to the southern telescope provided valuable experience that made the commissioning of the remote southern facility uneventful. The nearly identical nature of the two facilities streamlined operations and scheduling and ultimately aided in delivering uniform data products. Modular spare parts were available at both sites for most of the data acquisition hardware and for the more vulnerable components of the telescope hardware. These spares were rarely used. During the years of operation of the two facilities only 5 days were lost to equipment failure when a dome drive gear failed at Cerro Tololo and a part had to be shipped from the United States. A gradually failing array in the northern camera was replaced without loss of operations time during the monsoon shutdown period in 1999 August.

7.3. *Automated Data Acquisition and Intelligent Scheduling*

The 2MASS telescope operators supervised the automatic operation of the facilities. The telescope operators had responsibility for opening and closing the facility, monitoring the weather for conditions that might be hazardous to the telescope, maintaining the instrument cryogens, and writing and delivering the raw data tapes. The 2MASS computers, accounting for feedback from previous sky coverage, selected tiles for observation, pointed the telescope, and acquired data throughout the night. The scheduling software arranged for continuous observations from dusk to dawn spaced such that observations began and ended with standard star tiles. The scheduling algorithm accounted for the availability of each sky tile near its optimum air mass for observation, increasing priority for tiles that would soon be lost for the season. As a result, the telescopes did not experience periods when no observable tiles were available until the last several months of operations.

7.4. *Dynamic Range Extension*

2MASS developed a robust set of flux extraction algorithms that were effective even for heavily saturated objects. By adjusting the reset timing of the arrays to match the frame timing, both readouts constituting a "doubly correlated" frame contained calibratable information on 1.3 s and 51 ms timescales. The brightest unsaturated sources in the 1.3 s exposures overlapped with the faintest detectable sources in the 51 ms exposures providing continuous unsaturated flux estimation from the $\sim$17 mag detection limit to the $\sim$4 mag saturation limit of the 51 ms frames. As part of the evolution of the data reduction pipeline, a module was added for final processing that estimated fluxes with 10%–20% accuracy from the wings of sources that saturated even the 51 ms exposures. This algorithm successfully estimated the flux of the brightest infrared stars (mag ~ -4). The dynamic range of 2MASS spanned more than 20 mag.

7.5. *Source Detection Redundancy*

2MASS benefited substantially from multiple observations of sources on a variety of timescales. Every point in a 2MASS scan was imaged six, and occasionally seven, times in succession separated by the 1.455 s frame interval. For sources bright enough to be detectable in the 1.3 s single-frame exposure time, these multiple detection opportunities provided a robust means to discriminate between real sources and spurious events such as cosmic rays or unstable pixels.

The survey tiles overlapped 50″ in the right ascension direction and 8.′5 in declination. The independent measurements of sources in these overlap regions provided (1) checks for clouds during the intervals between calibration observations; (2) general tests of photometric stability, completeness, and reliability spanning the duration of the survey; and (3) a means of transferring astrometric information across tiles, which was of particular value for tiles containing few astrometric reference stars.

Calibration tile scans provided hundreds, and in some cases more than 3000, independent observations of 35 $1^\circ \times 8.'5$ fields. Each calibration tile contained hundreds of stars. The tiles were distributed uniformly around the sky and sampled a wide variety of astrophysical environments including low and high star density fields, star-forming regions, dark clouds, and galaxy clusters. The large number of repeated observations provided robust statistics for validating the source uncertainties assigned by the profile-fit and aperture photometry algorithms, as well as for estimating the survey's overall completeness.

Most importantly, calibration tile observations were obtained in sets of six consecutive scans. The rms statistics for the stars in each set provided a real-time characterization of the sensitivity of the observing system as a function of sky background, seeing, and system throughput. The sensitivity of the primary survey tiles was then established using the seeing and background relationships derived from the calibration observations.

7.6. *Quality Assurance Feedback*

The survey's large data rate and volume made it impossible for a human to validate every image. Instead, an automated quality assurance system produced feedback to support both survey planning and verification of the scientific quality of the data products. This system collected status outputs from each of the data reduction pipeline subsystems and produced a concise, web-based report for human review. For each scan the report summarized the achieved photometric and astrometric performance, as well as a number of telescope and camera metrics. A quality assurance scientist reviewed each nightly report and verified the overall numerical quality "score" that the pipeline assigned to each survey scan.

Because a portion of the sky might rapidly become inaccessible following observation, rapid feedback of the quality score to the observatory scheduling algorithm was essential. Before the pipeline was capable of processing full nights of data at the rate they were arriving from the telescopes, a "quick look" quality feedback pipeline processed each night's standard star tile observations ($\sim$10% of the data volume) and identified poor-quality data to be queued for reobservation. In the last year of operations the 2MAPPS pipeline became sufficiently mature that quality assessment could be conducted rapidly on the survey scans themselves, permitting direct assignment of a quality score for each completed scan and enabling reobservation of any tiles that fell below the requirements for sensitivity or image quality.

7.7. *Evolving Pipeline and Incremental Data Releases*

Although the prototyping campaign provided a well-informed starting point for the development of the 2MASS data reduction pipeline, the survey's requirements were far more rigorous (Table 1). Recognizing that achieving the high standards of spatial uniformity, completeness, and reliability would require substantial experience with significant amounts of real survey data, 2MASS planned for phased pipeline development and data product releases. Observations began with a preliminary version of the data reduction pipeline in place that provided basic source extraction data for analysis of the system's performance. The pipeline was allowed to evolve during the survey, incorporating improving knowledge of the observing systems, atmosphere, and near-infrared sky. Now obsolete "incremental" public data releases were generated from the output of this evolving pipeline. These data releases provided substantial experience in selecting highly reliable and complete subsets from the larger databases of source extractions and enabled scientists from the broader community to exercise these preliminary data products.

By the end of observations the data reduction pipeline had evolved to a final stable version. This final version incorporated instrumental calibrations and algorithms for photometry, astrometry, and image artifact identification that were optimized using all survey data. Final photometric calibration, for example, made use of a network of primary and secondary standard stars that were developed using the results of the preliminary processing. Similarly, the Tycho-2 catalog, which was not available during most of the survey, was available for use in the final pipeline. The entire survey data set was reprocessed using this final version of the pipeline, and the images and source extractions from final processing comprise the Atlas and Catalogs of the 2MASS All-Sky Data Release.

7.8. *Extended Mission Products*

The "working" databases from which the release catalogs were drawn contain 1.3 billion sources, many of which are redundant detections from repeated scans or scan overlaps, faint sources that fell below the thresholds for inclusion into the catalogs, or spurious sources extracted from the noise. Following the release of the primary products the 2MASS project entered an "extended mission" phase with the objective of delivering the contents of the working databases, calibration databases, and all Atlas Images to the public. These databases contain multiple detections of sources that range from duplicate detections of sources in the overlap between tiles to more than 3000 independent observations of sources in some calibration tiles. The extended mission will compute merged source statistics for every multiple detection providing a best estimate of flux and position for each multiply detected source. During the final year of 2MASS operations, a "deep" observing program filled idle time when all of the available sky had been observed. The exposure time for these deep observations was 46.8 s, or 6 times the standard 2MASS exposure time, producing data that were about 1 mag more sensitive. The deep observations covered 580 $\deg^2$ toward star-forming regions, galaxy clusters, M31, M32, the Pleiades, and the Lockman Hole (Beichman et al. 2003), as well the entire Large and Small Magellanic Clouds. Atlas Images and extracted source databases from these deep observations will also be released as part of the 2MASS extended mission.

8. SUMMARY

2MASS has produced a fiducial image of the near-infrared *J*- (1.25 μm), *H*- (1.65 μm), and K_s-band (2.16 μm) sky with

millijansky sensitivity supported by precise pipeline-extracted photometry and astrometry from a catalog of 471 million objects. The point-source S/N = 10 limit is achieved at or fainter than $J = 15.8$, $H = 15.1$, and $K_s = 14.3$ mag for virtually the entire sky. For sources at or above the S/N = 10 threshold the 2MASS Point Source Catalog is highly complete (>0.99) and reliable (>0.9995). Bright source photometric accuracy is <0.03 mag, and astrometric uncertainty is $\sim 0\farcs1$ relative to the ICRS. The images, catalogs of point and extended sources, and ancillary tables are publicly available via the 2MASS All-Sky Data Release.[27]

2MASS was enabled and executed through the work and dedication of hundreds of individuals whose contributions were instrumental to the design, fabrication, and operation of the observatories, cameras, and data systems and ultimately the processing and delivery of the survey's results to the astronomical community. Many of these individuals, institutions, and companies are identified in the 2MASS Explanatory Supplement.[28] The project is particularly indebted to Susan Kleinmann who made fundamental contributions to the initiation and design of 2MASS. Fred Gillett, Frank Low, Keith Matthews, and Gerry Neugebauer were also prime contributors to the work of transforming 2MASS from concept to reality. Many 2MASS participants gained substantial experience in survey work and pipeline data processing via their contributions to the *IRAS* survey. Indeed, 2MASS was constructed on a foundation that derives from the *IRAS* experience and owes a substantial debt to the designers and executors of that groundbreaking infrared survey. The 2MASS development, operations, data analysis, and archiving were funded by the National Aeronautics and Space Administration (NASA) and the National Science Foundation (NSF). Proof-of-concept and prototyping activities for 2MASS were supported by funds from the Air Force Offices of Scientific Research and the Air Force Geophysics Laboratory. The US Naval Observatory provided partial funding for the Mount Hopkins telescope. 2MASS was a joint project of the University of Massachusetts and IPAC (California Institute of Technology). The University of Massachusetts was responsible for the overall management of the project, the observing facilities, and the data acquisition. IPAC was responsible for data processing, data distribution, and data archiving. Observing facilities at Mount Hopkins and Cerro Tololo were operated by the Smithsonian Astrophysical Observatory and the National Optical Astronomy Observatory, respectively. The 2MASS project is deeply indebted to the 2MASS External Review Board (Michael Hauser [Chair], Gerry Neugebauer, Judith Pipher, Michael Strauss, and Nicholas White) for its service in reviewing the progress of the 2MASS project and the quality of its data products.

[27] See http://www.ipac.caltech.edu/2mass/releases/allsky/.
[28] See http://www.ipac.caltech.edu/2mass/releases/allsky/doc/sec1_7a.html.

REFERENCES

Bahcall, J. N., et al. 1991, The Decade of Discovery in Astronomy and Astrophysics (Washington: National Academy Press)
Beichman, C. A., Chester, T., Skrutskie, M., Low, F. J., & Gillett, F. 1998, PASP, 110, 480
Beichman, C. A., Cutri, R., Jarrett, T., Stiening, R., & Skrutskie, M. 2003, AJ, 125, 2521
Carpenter, J. 2001, AJ, 121, 2851
Cohen, M., Wheaton, W. A., & Megeath, S. T. 2003, AJ, 126, 1090
Cutri, R. M., et al. 2003, Explanatory Supplement to the 2MASS All Sky Data Release (Washington: NASA), http://www.ipac.caltech.edu/2mass/releases/allsky/doc/explsup.html
Fukugita, M., Ichikawa, T., Gunn, J. E., Doi, M., Shimasaku, K., & Schneider, D. P. 1996, AJ, 111, 1748
Gardner, J. P., Sharples, R. M., Frenk, C. S., & Carrasco, B. E. 1997, ApJ, 480, L99
Glazebrook, K., Peacock, J. A., Collins, C. A., & Miller, L. 1994, MNRAS, 266, 65
Hög, E., et al. 2000, A&A, 357, 367
Jarrett, T. H., Chester, T., Cutri, R., Schneider, S. E., & Huchra, J. P. 2003, AJ, 125, 525
Jarrett, T. H., Chester, T., Cutri, R., Schneider, S., Skrutskie, M., & Huchra, J. P. 2000, AJ, 119, 2498
Johnson, H. L. 1962, ApJ, 135, 69
Milligan, S., Cranton, B. W., & Skrutskie, M. F. 1996, Proc. SPIE, 2863, 2
Neugebauer, G., & Leighton, R. B. 1969, Two Micron Sky Survey, a Preliminary Catalog (NASA SP-3047; Washington: GPO)
Nikolaev, S., Weinberg, M. D., Skrutskie, M. F., Cutri, R. M., Wheelock, S. L., Gizis, J. E., & Howard, E. M. 2000, AJ, 120, 3340
Persson, E., Murphy, D. C., Krzeminski, W., Roth, M., & Rieke, M. J. 1998, AJ, 116, 2475
White, R. L., Postman, M., & Lattanzi, M. G. 1992, in Digitised Optical Sky Surveys, ed. H. T. MacGillivray & E. B. Thompson (Dordrecht: Kluwer), 167
York, D. G., et al. 2000, AJ, 120, 1579
Zacharias, N., et al. 2000, AJ, 120, 2131